1
Synthesis and Functionality of Substituted Polyacetylenes

Jianzhao Liu, Jacky W. Y. Lam, and Ben Zhong Tang
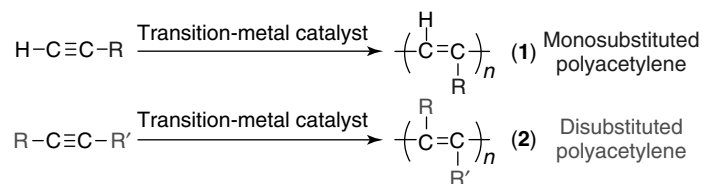
1.1
Introduction

Polyacetylene (PA) is the archetypal conjugated polymer. The seminal discovery of the metallic conductivity of its doped form has triggered a huge surge of interest in conductive polymers and has spawned an exciting area of research on synthetic metals.[1] As a result of rapid advances in the area, we are now on the threshold of a ''plastic-electronics era'' that previously could only be imagined in science fiction.

Structurally, PA is a linear polyene chain $[-(HC=CH)_n-]$. The existence of two hydrogen atoms in its repeat unit offers ample opportunity to decorate the backbone with pendants: replacement of hydrogen in each repeat unit by one or two substituents yields mono- (**1**) and disubstituted PAs (2), respectively (Scheme 1.1). The pendant and backbone can interact with each other: for example, the former perturbs the electronic conjugation of the latter, while the latter influences the molecular alignment of the former. Proper structural design may tune the backbone–pendant interplay into harmony and synergy, generating new substituted PAs with novel functionalities. While PA is electrically conductive, introduction of such pendant as mesogen, chromophore, photosensitive double bond, or naturally occurring building block may endow it with such new functional properties as electro-optic activity, photonic responsiveness, and biologic compatibility.

Considerable efforts have been devoted to the synthesis of the substituted PAs and study of their properties [1–9]. Attachment of polar groups to the polyene backbone enables the integration of functional pendants into the PA chain through various functional-group transformations, which was, however, a difficult task at the early stage of PA chemistry. Difficulties were ascribed to the poisoning of the metathesis catalysts by the functional groups [10, 11]. The later discovery of the functionality-tolerant organorhodium catalysts was a thrilling advance in the

1) Heeger, MacDiarmid, and Shirakawa won the Nobel Prize in Chemistry in 2000 for their pioneer work in the area.

$$H-C\equiv C-R \xrightarrow{\text{Transition-metal catalyst}} \left(\!\!\begin{array}{c} H \\ | \\ C=C \\ | \\ R \end{array}\!\!\right)_{\!n} \quad \textbf{(1)} \quad \begin{array}{l}\text{Monosubstituted}\\\text{polyacetylene}\end{array}$$

$$R-C\equiv C-R' \xrightarrow{\text{Transition-metal catalyst}} \left(\!\!\begin{array}{c} R \\ | \\ C=C \\ | \\ R' \end{array}\!\!\right)_{\!n} \quad \textbf{(2)} \quad \begin{array}{l}\text{Disubstituted}\\\text{polyacetylene}\end{array}$$

Scheme 1.1 Polymerizations of mono- and disubstituted acetylenes.
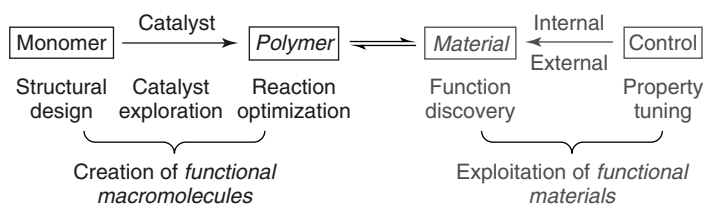
Chart 1.1 Development of polyacetylene-based functional macromolecules and materials.

area [12, 13], but the catalysts work for only limited types of monomers (e.g., phenylacetylene derivatives and monosubstituted 1-alkynes) through an insertion mechanism [14]. The syntheses of functional PAs via the metathesis route remained difficult, with the polymerizations of disubstituted functional acetylenes being particularly intractable.

Our research group has worked on PA functionalization through a systematic approach. Our efforts have covered design of monomer structures, exploration of new catalysts, optimization of reaction conditions, discovery of functions, and manipulation of properties by internal and external means (Chart 1.1). Our strategy has worked well and we have generated a wide variety of new PA-based functional macromolecules and materials. In this chapter, we briefly summarize our efforts and results on the development of the new functional PAs.

1.2
Polymer Syntheses

1.2.1
Catalysts

In general, in the presence of Ziegler–Natta catalysts, the pure PA was obtained as an intractable black powder that is very difficult to make into samples of a shape suitable for measurement of spectra and physical properties because of its insolubility, infusibility, and instability. To address the processability and stability problem encountered by unsubstituted PA and explore new functionalities, polymer scientists tried to synthesize functionalized substituted PAs. This task is critically dependent
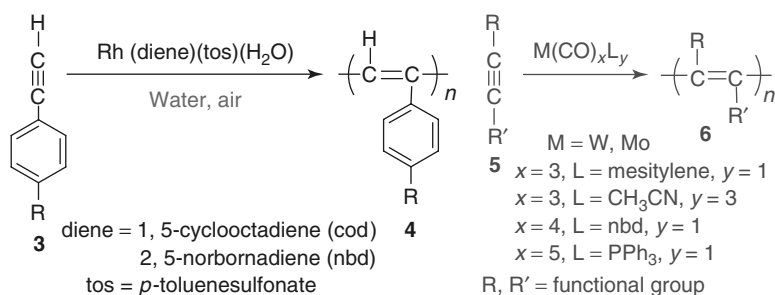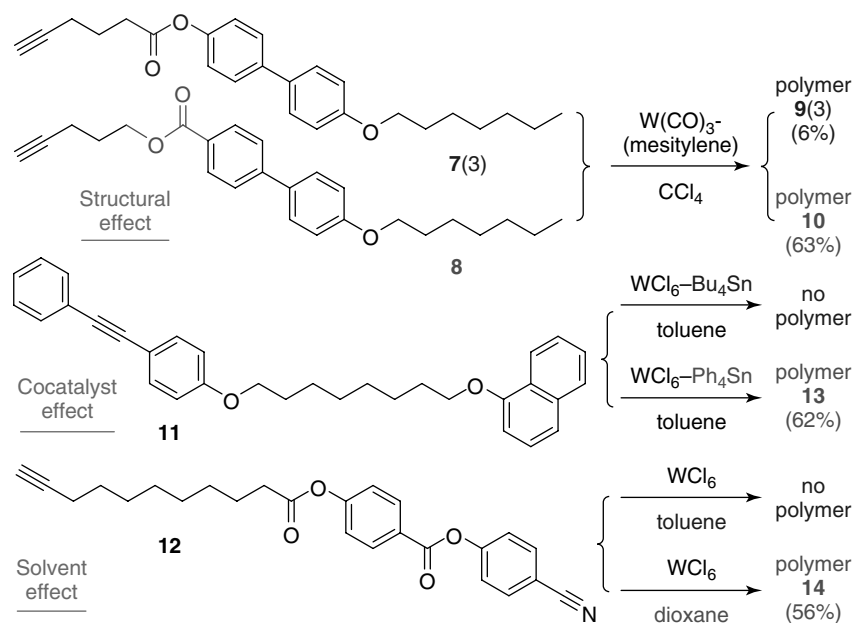
Scheme 1.2 Polymerizations of acetylenes by water-soluble
Rh and air-stable Mo, and W-based carbonyl complexes.

on the exploration of effective catalysts. At an early stage, polymerization of substituted acetylenes was studied by using conventional Ziegler–Natta catalysts aiming at synthesizing processable and functional PAs [4]. However, many attempts led to the conclusion that only sterically unhindered monosubstituted acetylenes can be polymerized to give insoluble polymers and/or soluble oligomers. Traditional ionic and radical initiators were known to be inefficient to polymerize substituted acetylenes. Later, Mo, W, Ta, and Nb-based metathesis catalysts were successfully developed [1, 3, 7, 11]. The main difficulty with these systems was the ''incompatibility'' of the polar groups with these metathesis catalysts. The functionality tolerance of the Rh-based insertion catalysts thus attracted our attention. To expand the variety of the Rh catalysts, we prepared a series of Rh complexes Rh(diene)L (L = ligand). Importantly, we have developed a catalyst system that can initiate acetylene polymerizations in water and air, giving stereoregular polymers (**4**) in high yields (Scheme 1.2) [15].

Like their older versions, the new Rh catalysts are also only effective for the polymerizations of specific types of monomers. To develop more general systems, we turned our attention back to metathesis catalysts. $MoCl_5$ and WCl_6 are classical metathesis catalysts, but the early attempts to use them to polymerize functional acetylenes often resulted in the formation of insoluble or oligomeric products in low yields. We envisioned that the metal halides would be functionality tolerant, for they could cyclopolymerize functional diynes into cyclic polyenes [5]. Our prediction proved correct: through catalyst–substrate matching and reaction-condition optimization, we accomplished our goal of using the metal halides to catalyze the linear polymerizations of various functional acetylenes.

The metal halides are, however, air- and moisture-sensitive. In 1989, Tang found that several stable metal carbonyl complexes catalyzed the polymerizations of nonfunctional 1-alkynes. We extended his effort in the area and prepared a series of $M(CO)_x L_y$ complexes. Delightfully, many functional acetylenes (**5**) could be polymerized by these metal carbonyl complexes (Scheme 1.2) [16].

Scheme 1.3 Effects of substrate, cocatalyst, and solvent on acetylene polymerizations.

1.2.2
Polymerization Behaviors

In order to match the catalysts with particular substrates, we prepared hundreds of functional acetylenes. The substrate–catalyst matching is structurally sensitive: a seemingly subtle variation in the functional group can greatly influence the behavior of polymerization of a monomer by a given catalyst. For example, **7**(3) and **8** differ only in the orientation of the ester unit but show distinct polymerizability by W(CO)₃(mesitylene): **8** can be effectively polymerized but **7**(3) cannot (Scheme 1.3) [16]. Polymerization conditions (cocatalyst, solvent, etc.) can affect the fate of a specific substrate–catalyst pair. For instance, **11**–WCl₆ may be a bad or good combination, depending on whether tetra(*n*-butyl)tin or tetraphenyltin is used as a cocatalyst [17]. Polymerization of **12** does not occur at all in toluene but proceeds well in dioxane.

In general, rhodium catalysts can efficiently polymerize various monosubstituted acetylenes (e.g., phenylacetylene and 1-alkyne derivatives with polar groups) to give polymers with high molecular weights (MWs). However, the polymerization of highly polar monomers, particularly those with acidic protons, is still a difficult proposition. For example, polymerization of acetylenic monomers containing carboxy groups has been a daunting job. The direct polymerization of 4-ethynylbenzoic acid was deemed very difficult, if not impossible. Our group has succeeded in direct polymerizations of a series of highly polar phenylacetylene derivatives. The
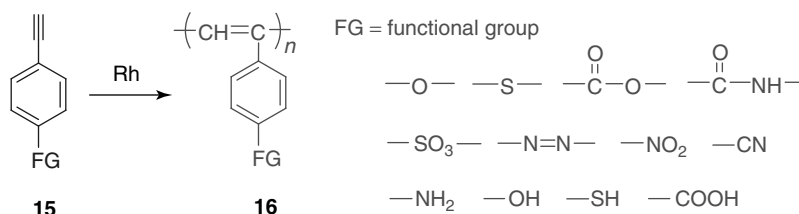
Scheme 1.4 Polymerization of functionalized acetylenes.

polymerizations of phenylacetylene derivatives **15** (Scheme 1.4) with various polar groups (e.g., oxy, carboxyl, hydroxyl, azo, cyano, thiol, amino, and nitro) catalyzed by organorhodium complexes, [Rh(cod)Cl]$_2$ (cod = 1,5-cyclooctadiene), [Rh(nbd)Cl]$_2$, and Rh$^+$(nbd)[C$_6$H$_5$B$^-$(C$_6$H$_5$)$_3$] (nbd = norbornadiene), afforded corresponding polymers **16** with high MWs (M_w up to 488 500) and low polydispersity indexes (PDIs = M_w/M_n, down to 1.03, where M_n and M_w stand for number and weight-average MWs) [1, 2, 18].

As a result of optimization of the polymerization reactions, many functional monomers are transformed into polymers of high MWs (up to several million) in high yields (up to 100%). Substituted PAs containing various functional groups (e.g., crown ether, sulfonate, amide, dipeptide, saccharide, nucleoside, sterol, cyano, thiophene, vinyl, phthalimide, indole, siloxane, and silole) have been obtained [1, 2]. Examples are given in Charts 1.2 and 1.3.

On the basis of our results, a substrate–catalyst matching map is drawn as shown in Chart 1.4. Functionalized 1-arylacetylenes are polymerizable only by the Rh-based catalysts, although their nonfunctional cousins can be polymerized by other catalysts. Polymerizations of functionalized 1-alkynes are effected by the W-based catalysts, with the Rh ones giving moderate results. Propiolates can be effectively polymerized by the Mo and Rh catalysts. The Rh complexes cannot polymerize disubstituted acetylenes. Polymerizations of alkyl 2-alkynoates and alkyl 3-arylpropiolates are effected by the Mo catalysts, while those of aryl 3-arylpropiolates, 1-aryl-1-alkynes, and diarylacetylenes are initiated by the W catalysts. While polymerization of monosubstituted acetylenes (Chart 1.4, nos. 1–3) normally proceeds at room temperature in polar solvents (e.g., dioxane), disubstituted acetylenes (nos. 4–8) generally polymerize at higher temperatures (e.g., ∼80 °C) in nonpolar solvents (e.g., toluene).

1.2.3
Polymer Reactions

Polymer reactions can be used as a tool to further functionalize the preformed acetylenic polymers or create functional polymers inaccessible by direct polymerizations. For example, the polymer **45** comprises hydrophobic poly(phenylacetylene) (PPA) skeleton and hydrophilic amine pendant. Because of this structural feature, the polymers are not soluble in common organic solvents as well as aqueous media. Ionization of **45** by hydrochloric acid furnishes polycation **46** (Scheme 1.5)
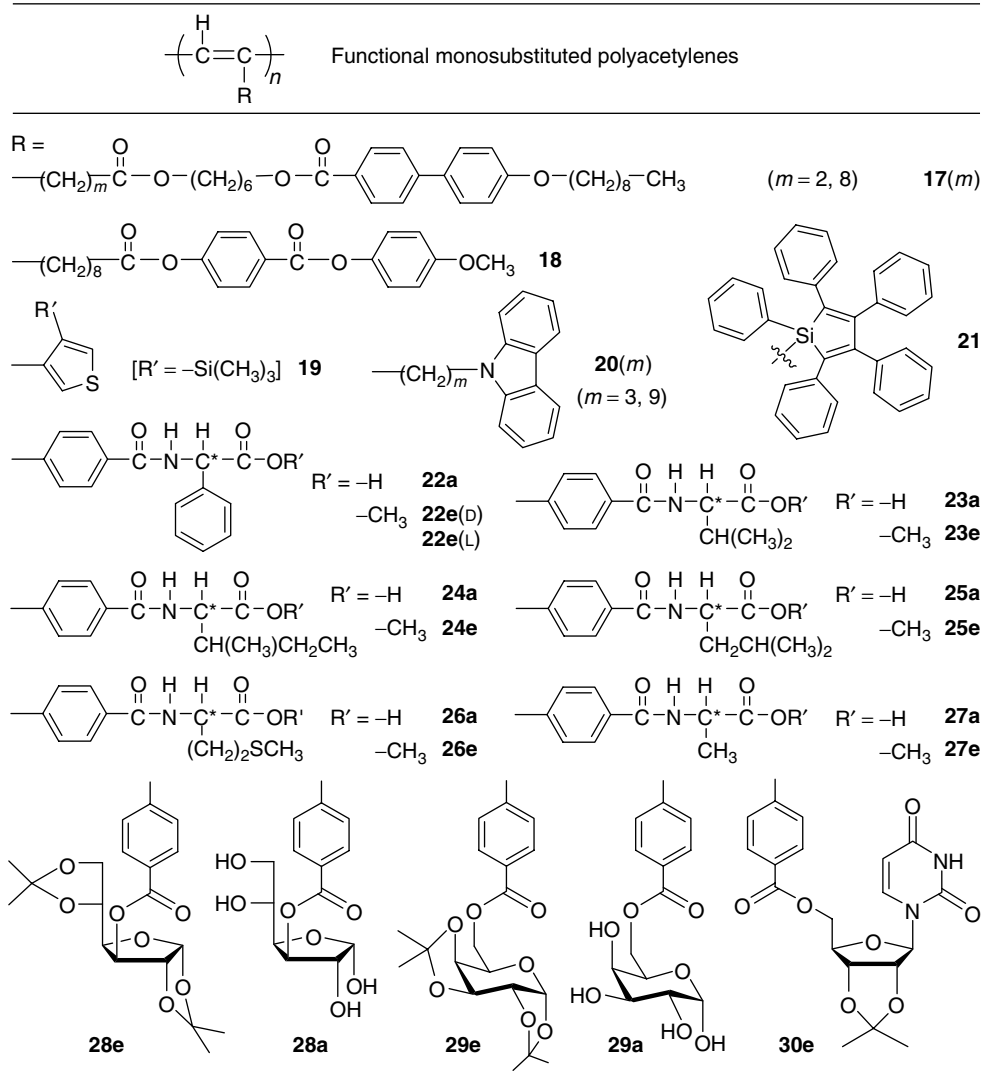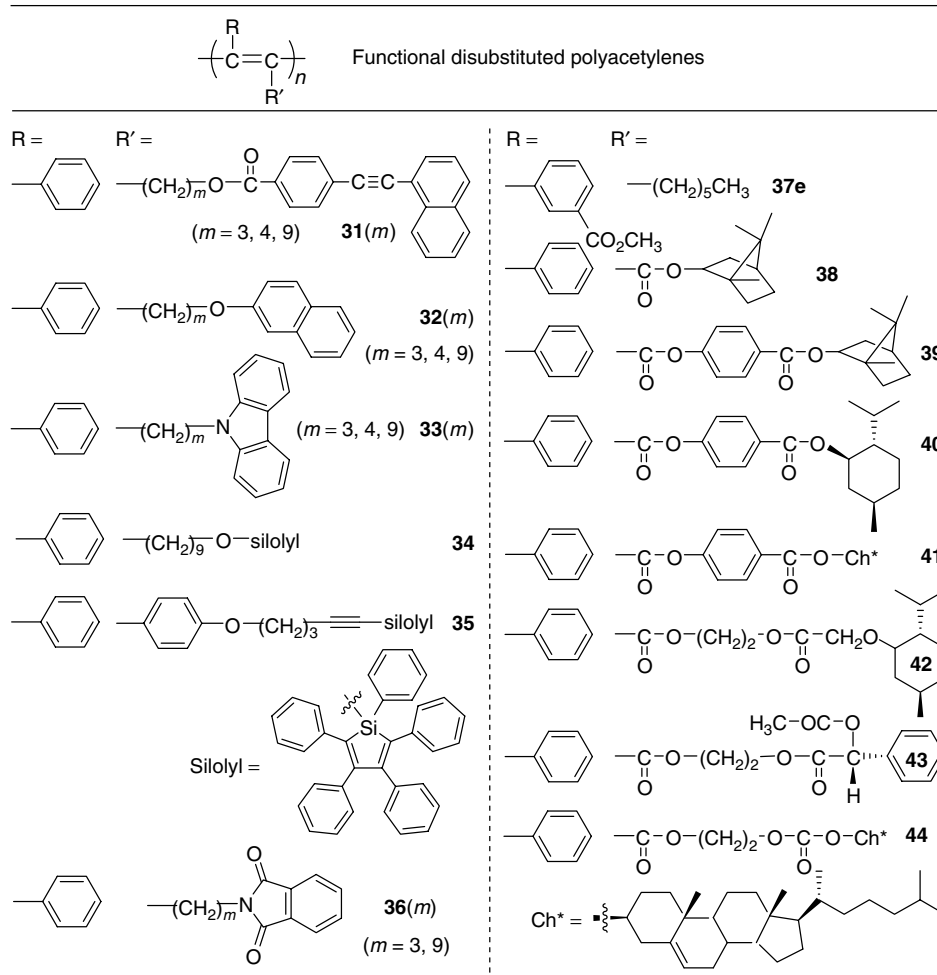
Chart 1.2 Examples of monosubstituted PAs.

[18], which is soluble in water. While polymer reactions normally do not proceed to 100% completion, surprisingly, cleaving the ether groups of **29e** by hydrolysis can give **29a** with cytocompatabile sugar pedants which do not contain any ether residue.

It should be noted that it is not possible to gain access to functionalized disubstituted PAs by the direct polymerizations, owing to the inherent intolerance of the metathesis catalysts to polar groups. However, polymer-reaction approach can address this problem. By click chemistry, many highly polar functional groups

Functional disubstituted polyacetylenes

$$\left(\!\!\begin{array}{c} R \\ | \\ C=C \\ | \\ R' \end{array}\!\!\right)_{\!n}$$

R =   R' =

—(CH$_2$)$_m$—O—C(=O)—C$_6$H$_4$—C≡C—naphthyl   (m = 3, 4, 9)   **31**(m)

—(CH$_2$)$_m$—O—naphthyl   **32**(m)   (m = 3, 4, 9)

—(CH$_2$)$_m$—N—carbazolyl   (m = 3, 4, 9)   **33**(m)

—(CH$_2$)$_9$—O—silolyl   **34**

—C$_6$H$_4$—O—(CH$_2$)$_3$—C≡C—silolyl   **35**

Silolyl =

—(CH$_2$)$_m$—N-phthalimide   **36**(m)   (m = 3, 9)

R =   R' =

—(CH$_2$)$_5$CH$_3$ **37e**

—C$_6$H$_4$(CO$_2$CH$_3$)—C(=O)—O—bornyl   **38**

—C(=O)—O—C$_6$H$_4$—C(=O)—O—bornyl   **39**

—C(=O)—O—C$_6$H$_4$—C(=O)—O—menthyl   **40**

—C(=O)—O—C$_6$H$_4$—C(=O)—O—Ch*   **41**

—C(=O)—O—(CH$_2$)$_2$—O—C(=O)—CH$_2$O—menthyl   **42**

—C(=O)—O—(CH$_2$)$_2$—O—C(=O)—C(OC(=O)CH$_3$)(H)—C$_6$H$_5$ **43**

—C(=O)—O—(CH$_2$)$_2$—O—C(=O)—O—Ch*   **44**

Ch* =

Chart 1.3 Examples of disubstituted PAs.

can be conveniently attached to disubstituted PA **48** to furnish **49** [19]. **47** and **37e** can undergo nucleophilic substitution and hydrolysis reactions, respectively, to provide imidazole- and carboxy-functionalized disubstituted PAs **50** and **37a** [20, 21]. Deprotection of imide **36**(9) yields amine **51**, which can further be ionized by hydrobromic acid to give polycation **52** [22, 23].

1.3
Functional Properties

The substituted PAs comprising conjugated backbones and functional pendants are expected to show unique properties. Studies of these properties will help

	Substrate		Catalyst		
No.	Acetylene monomer carrying functional group (FG)		Mo	W	Rh
1	H——≡——Ar—FG	1-arylacetylene	○	○	●
2	H——≡——$(CH_2)_m$—FG	1-alkyne	○	●	◐
3	H—≡—CO_2—FG	Propiolate	●	◐	●
4	$CH_3(CH_2)_{\overline{m}}$≡—$CO_2$—$(CH_2)_m$—FG	Alkly 2-alkynoate	●	○	○
5	Ar——≡—CO_2—$(CH_2)_m$—FG	Alkyl 3-arylpropiolate	●	○	○
6	Ar—≡—CO_2—Ar—FG	Aryl 3-arylpropiolate	○	●	○
7	FG—Ar—≡—$(CH_2)_m$—FG	1-aryl-1-alkyne	○	●	○
8	Ar——≡—Ar—FG	Diarylacetylene	○	●	○

Degree of substrate–catalyst matching: ● = excellent, ◐ = good, ○ = bad

Chart 1.4 Catalyst–substrate matching map.

understand how the polymers behave and aid our efforts to develop the new macromolecules for technologically useful materials. PA is notoriously intractable and unstable. In contrast, most of our functionalized PAs are soluble, thanks to the suppression of backbone interactions by the pendant groups. All the disubstituted PAs are very stable: for example, **32**(4) does not decompose when heated in air at high temperatures (e.g., 200 °C) for a prolonged time (e.g., 12 hours). The pendants shroud the polyene backbone, protecting it from thermolytic attack [24].

The functionalized poly(1-alkyne)s and polypropiolates are also stable. For example, **9**(3) does not degrade when it is heated in air at temperatures up to 200 °C (Figure 1.1a). Similarly, M_w of **9**(9) does not change when it is exposed to UV irradiation or stored in air (Figure 1.1b). Functionalized poly(1-arylacetylene)s, however, are only moderately stable and degrade when heated to >100 °C or stored under ambient conditions [17]. This makes them unsuitable for long-term uses but potentially attractive as materials that must decompose during and/or after use (e.g., photo- and biodegradable polymers).

1.3.1
Electrical Conductivity and Photoconductivity

The introduction of substituents onto the PA backbone has been proved to be an excellent solution to the problem of processability and stability. Nevertheless, the electrical conductivity of their doped form is usually much lower than that of doped PA, and still in the semiconductor region, which may be attributed to the twisted backbones forced by substituents and, hence, decreased overlap of π-orbitals.

Although the substituted PAs have the low absolute values of electrical conductivity, their relative conductivities are still higher than those of the conventional single-bonded polymers and may be further enhanced by external stimuli. Of
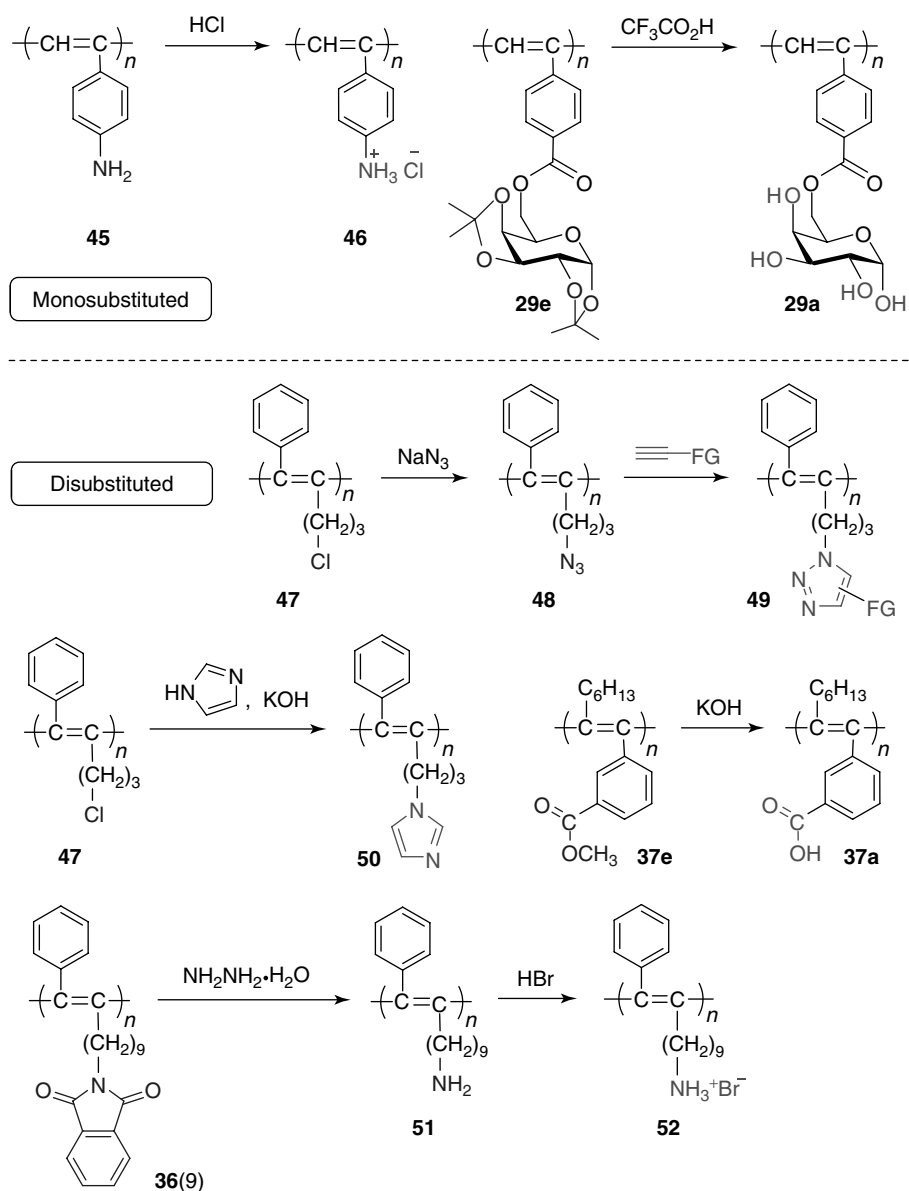
Scheme 1.5 Examples of polymer reactions.

particular interest and technological implication is the enhancement in electrical conductivity by photoirradiation, commonly known as *photoconductivity* (PC). Much work has been done on the photoconduction in substituted PAs [25]. It has been found that (i) the PAs containing electron-donating substituents exhibit higher PC than those with electron-accepting ones; (ii) the PC is further improved
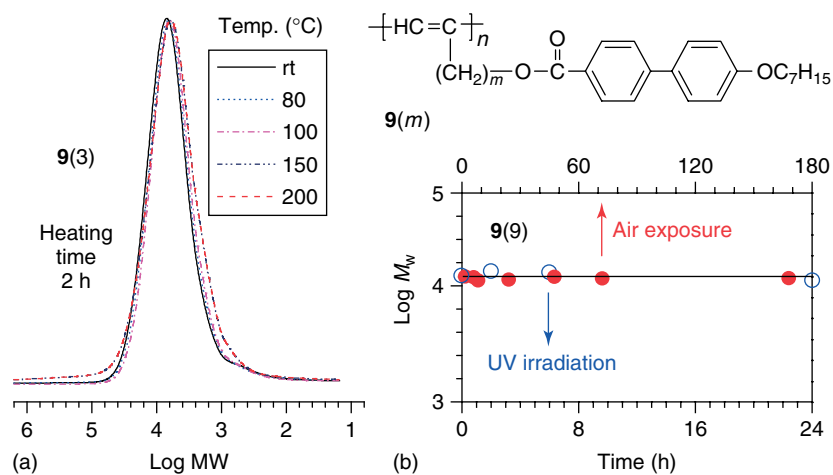
Figure 1.1 Resistances of **9**(*m*) against (a) thermolysis and (b) oxidation and photolysis in air.
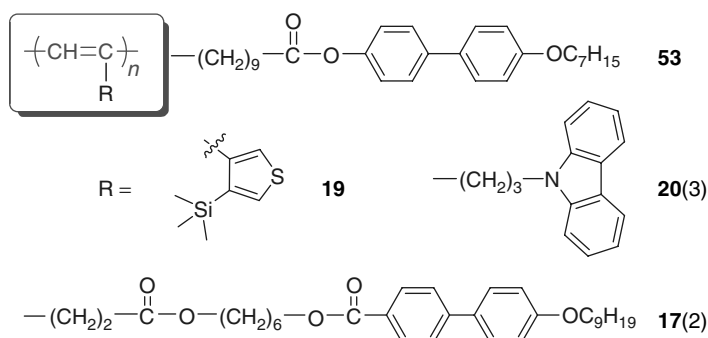
Chart 1.5 Examples of photoconductive PAs.

when the donor substituents are simultaneously good hole-transporters; and (iii) the photoconduction becomes more efficient when the donor substituents are mesogenic and can be packed in an ordered fashion.

Some examples of photoconductive PAs are shown in Chart 1.5. **19** and **20**(3) with donor substituents have high conductivity, with the value for latter one being higher because **20**(3) is simultaneously a good hole-transporter (Figure 1.2) [25]. A liquid crystalline polyacetylene (LCPA) is expected to have a high PC because of the high charge mobility in its closely packed mesogen phase. Interfaces between amorphous and mesogen phases also favor photoconductions, for excitons dissociate efficiently at, and carriers move rapidly along, the interfaces. Indeed, LCPA **53** shows higher PC than PPA, a non-LC photoconductor [26]. LCPA **17**(2) shows even higher PC, because of its better-ordered LC aggregates formed in the photoreceptor fabrication process.
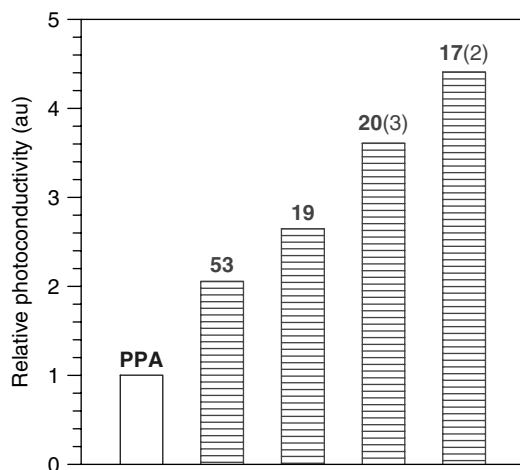
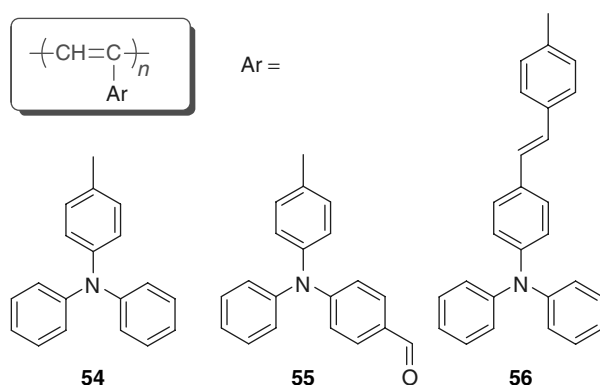**Figure 1.2** Photoconductivity of some selected PAs.

Chart 1.6 Triphenylamine-functionalized PAs.

Triphenylamine (TPA) is a typical donor and a famous building block for hole-transport materials. With an anticipation to obtain PAs with good photocon-duction performances, we incorporated TPA into PAs (Chart 1.6), which were used as chare-generation materials (CGMs) [27]. For example, the half-discharge time ($T_{1/2}$) of **54** is 0.09 seconds and the photosensitivity (*S*) is 1010.1 mm^2 mW^{-1} s^{-1}, which are quite high among substituted PAs. The photoreceptor with **55** as CGM shows a lower *S* value than the device based on **54**. This is easy to understand because the formyl group attached to the TPA moiety is electron withdrawing, which decreases the hole-transport efficiency. The photoreceptor with **56** as CGM gives the lowest *S* value among the three TPA-containing PAs. This result can be explained in terms of charge-generation efficiency. **56** has the highest fluorescence quantum efficiency among the polymers. This indicates that the photogenerated geminate pairs have a high probability to recombine. Consequently, the number of
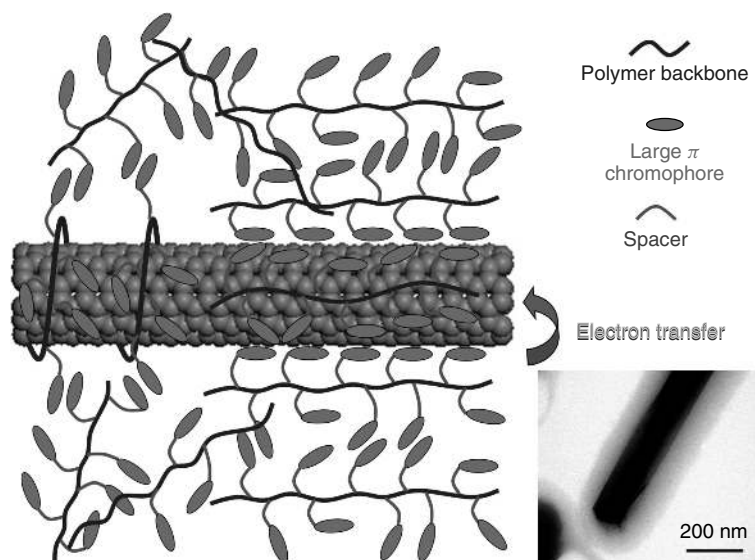
Figure 1.3 Schematic illustration of hybridization of CNT with PAs. Inset: TEM image of the hybrid of **54** and MWCNT.

the photogenerated free charges in the **56**-based photoreceptor becomes smaller, hence its observed low PC.

Like most conjugated polymers, substituted PAs can be considered as p-type semiconductors, and their hybridizations with n-type carbon nanotube (CNT) and inorganic semiconductors may offer nanohybrids with enhanced PC performances. Our group has found that substituted PAs bearing aromatic pendants can efficiently wrap CNTs and thus enhance the solubility. On the basis of our systematic study, the solubilization mechanism of CNTs may be summarized as sketched in Figure 1.3 [28–30]. The polymer chains may thread onto and/or wrap around the CNT shells due to strong $\pi-\pi$ stacking and donor–acceptor interaction of their aromatic pendants and conjugated backbones with the CNT wall surfaces. The polymer coating is thickened by the deposition of polymer chains via pendant–pendant electronic interactions and physical chain entanglements. The affinity of the polymer chains with the solvent molecules brings the polymer-coated or -wrapped CNTs into the organic solvent media, leading to the dissolution of CNTs.

Employing the p–n junction strategy and the CNT-solubilizing method mentioned above, we fabricated photoreceptor devices using PA/CNT nanohybrids as CGMs. As expected, the photoreceptor devices displayed improved PCs, in comparison to those of the devices based on the parent polymers. Amazingly, **55**/multiwalled carbon nanotube (MWCNT)-based photoreceptor shows a $T_{1/2}$ value as low as 0.01 seconds [27]. Its corresponding S value is as high as ∼9091 mm^2 mW^{-1} s^{-1}, about 40 times that of the **55**-based device. This dramatically enhanced PC is due to the MWCNT component in the photoreceptor. As

discussed above, the MWCNTs behave as an electron acceptor. The existence of the MWCNTs in the charge-generation layer improves charge-generation efficiency through a mechanism of photoinduced charge transfer from **55** to MWCNTs (Figure 1.3). Meanwhile, the MWCNTs offer one-dimensional electron-transport channels. Their conductive networks quickly transport the photogenerated electrons to the surface of the photoreceptor to neutralize the surface charge, thus resulting in steeply decreased surface potential and transiently short $T_{1/2}$ value. The device with **54**/MWCNT hybrid as CGM also shows enhanced PC, but the enhancement is less than that for the **55**/MWCNT-based device.

Nanohybridization of inorganic semiconductors with organic conjugated PAs offers the possibility to create new hybrids with combined advantages of the two components, that is, the high charge mobility of the inorganics and the ready processability of the organics, which may serve as active materials in the fabrication of photoreceptors. With great efforts, we developed a facile strategy for the hybridization of CdS nanorods with PPA chains. Utilizing an approach of "pre-assembly plus copolymerization," [31] CdS–PPA nanohybrid **59** has successfully been prepared (Figure 1.4). This hybrid is completely soluble in common organic solvents and can form homogeneous films when its solutions are cast on solid substrates. Because of the high solubility and film-forming capability of the hybrid, a series of **59**-based photoreceptors were prepared by a solution-casting process and their PCs were evaluated. One of the devices shows a $T_{1/2}$ value of 2.63 seconds and an S value of 34.3 mm^2 mW^{-1} s^{-1}, which are better than those of all the devices using the parent form of PPA ($T_{1/2} = 3.67$ seconds and $S = 24.5$ mm^2 mW^{-1} s^{-1}) and CdS ($T_{1/2} = 4.74$ seconds and $S = 19.0$ mm^2 mW^{-1} s^{-1}) as well as their physical blend PPA/CdS ($T_{1/2} = 4.30$ seconds and $S = 21.0$ mm^2 mW^{-1} s^{-1}) as CGMs.

Similarly, functional perovskite hybrid **60** generated between PA ammonium **52** and PbBr$_2$ shows a better photoconduction result than its parent polymer **52** (Scheme 1.6) [22]. The PC performance of the photoreceptor of **52** is poor, as evidenced by its high $T_{1/2}$ (10 seconds) and low S (9.1 mm^2 mW^{-1} s^{-1}) values. In the solid film, the ammonium cations and bromide anions of the polysalt form a network of randomly distributed electrostatic centers. The photogenerated charges are readily attracted to, and detained by, the network of the ions, which reduces their likelihood of contributing to photoconduction. When **52** is hybridized with lead bromide, its once-free ammonium cations now become confined in an ordered fashion through their coordination with the sheets of the corner-sharing metal halide octahedrons. The interactions between the fixed ions anchored to the inorganic frameworks and the mobile charges photogenerated on the conjugated PA backbones are weaker than those in the polysalt film. Some of the charges may find their paths to the electrode to discharge the surface potential. As a result, the hybrid **60** displays an improved PC performance ($T_{1/2} = 3.96$ seconds and $S = 23.0$ mm^2 mW^{-1} s^{-1}), in comparison to its polysalt precursor.
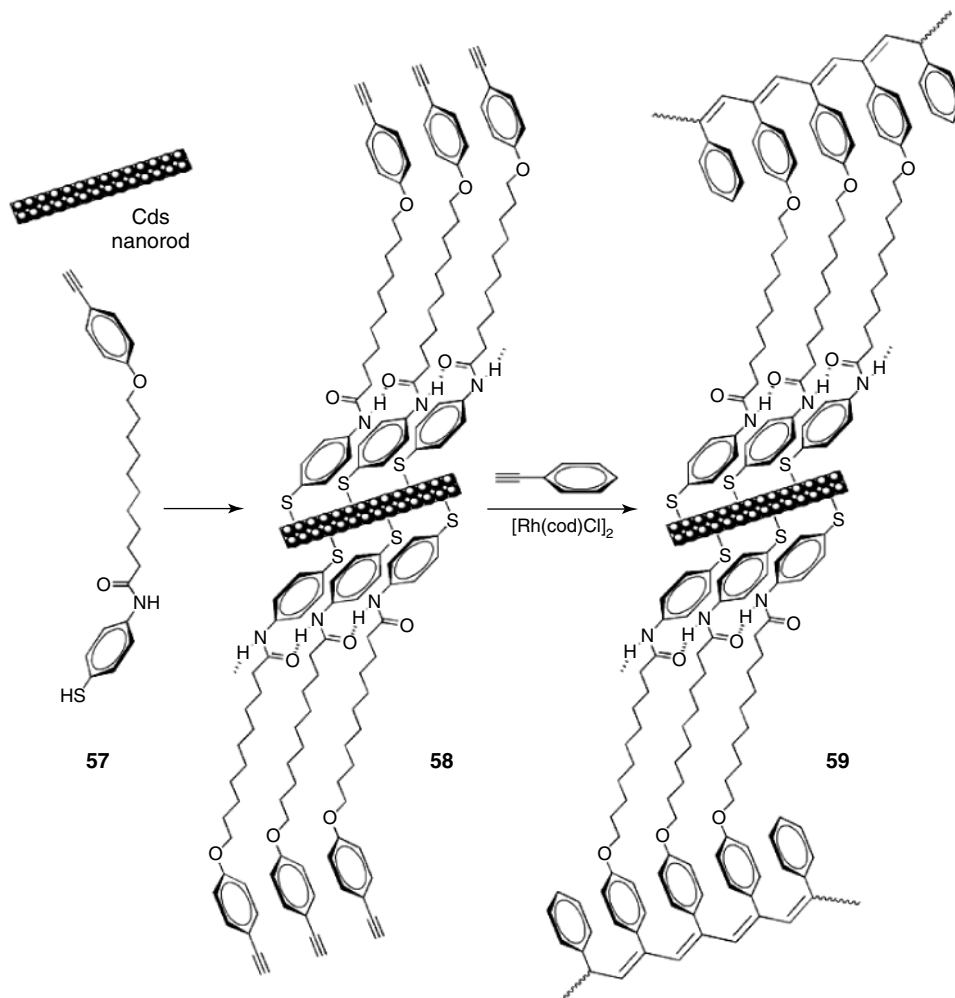
Figure 1.4 Assembly of the molecules of monomer **57** on the surface of CdS nanorod gives composite **58**, whose copolymerization with phenylacetylene yields CdS–PPA hybrid **59**.

1.3.2
Liquid Crystallinity

Liquid crystals and PAs are optically and electronically active, respectively; melding the two at molecular level may spawn LCPA hybrids with both optical and electronic activities. The LCPAs may also be third- and second-order nonlinear optically (NLO) susceptible because conjugated polymer chains and polarized mesogenic groups, are respectively, $\chi^{(3)}$- and $\chi^{(2)}$-active. The common recipe for the structural design
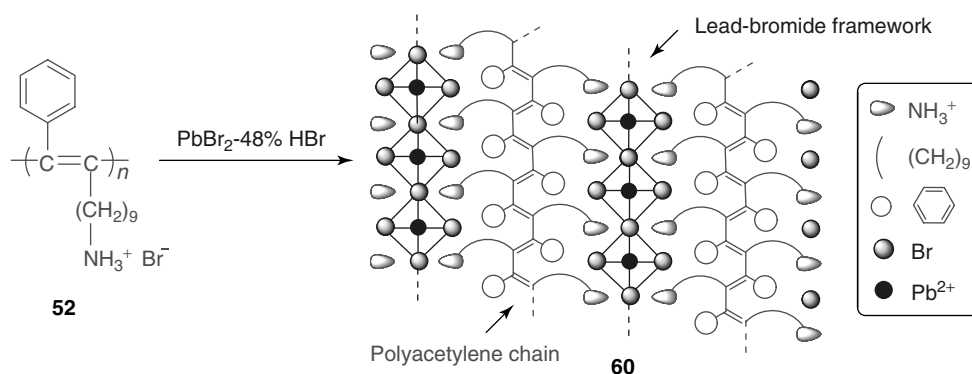
Scheme 1.6 Preparation of PA–perovskite hybrid.

of side chain LC polymers has been ''mesogenic pendant + flexible backbone.'' Rigid polymer backbones have generally been believed to be detrimental to the packing arrangements of the mesogens in the side chains. As a result of this general belief, LC polymers with rigid backbones have seldom been developed. The study of LCPAs with rigid polyene backbones is of interest, and successful development of such polymers may open a new avenue for the exploration of new types of LC polymers and help deepen our understanding on liquid crystals. Since stiff-chain polymers can be oriented by external forces, the LCPAs may show anisotropic mechanical properties, which may contribute to the search for high-performance engineering materials.

Inspired by these attractive prospects, many research groups have worked on the development of LCPAs. Through careful design of flexible spacers, functional bridges, mesogenic cores, and functional tails, we have synthesized a series of highly soluble and thermally stable mono- and disubstituted thermotropic LCPAs and systematically studied their LC behaviors [1, 2, 32–38]. Typical examples are shown in Chart 1.7. We have systematically studied their LC behaviors, especially the structure–property relationships in the LCPA systems. The packing arrangements in the mesophases of the LCPAs and their mesomorphic transitions have been found to vary with the molecular structures of their mesogenic pendants. Some examples of the structure–property relationships are given in Table 1.1.

Polymer **64** is a poly(1-phenyl-1-alkyne) derivative containing a mesogenic unit with a biphenyl (BP) core. It displays an S_A mesophase in the temperature range of 172−158 °C when cooled from its isotropic melt. Its cousin with a phenylcyclohexyl core (**65**) exhibits a nematic (N) mesophase at much lower temperatures (108−90 °C), although it differs from **64** by one ring structure in the mesogenic core (cyclohexyl in **65** versus phenyl in **64**). Polymers **62** and **63** have almost identical molecular structures, expect for that the former and latter have ester and ether bridges, respectively. This seemingly subtle structural difference affects the mesogenic packing arrangements, with the former ordered in a bilayer structure in an interdigitated fashion, namely, interdigitated smectic A phase (S_{Ad}), while the latter packs in a monolayer structure (S_A; Table 1.1, nos. 3 and 4).
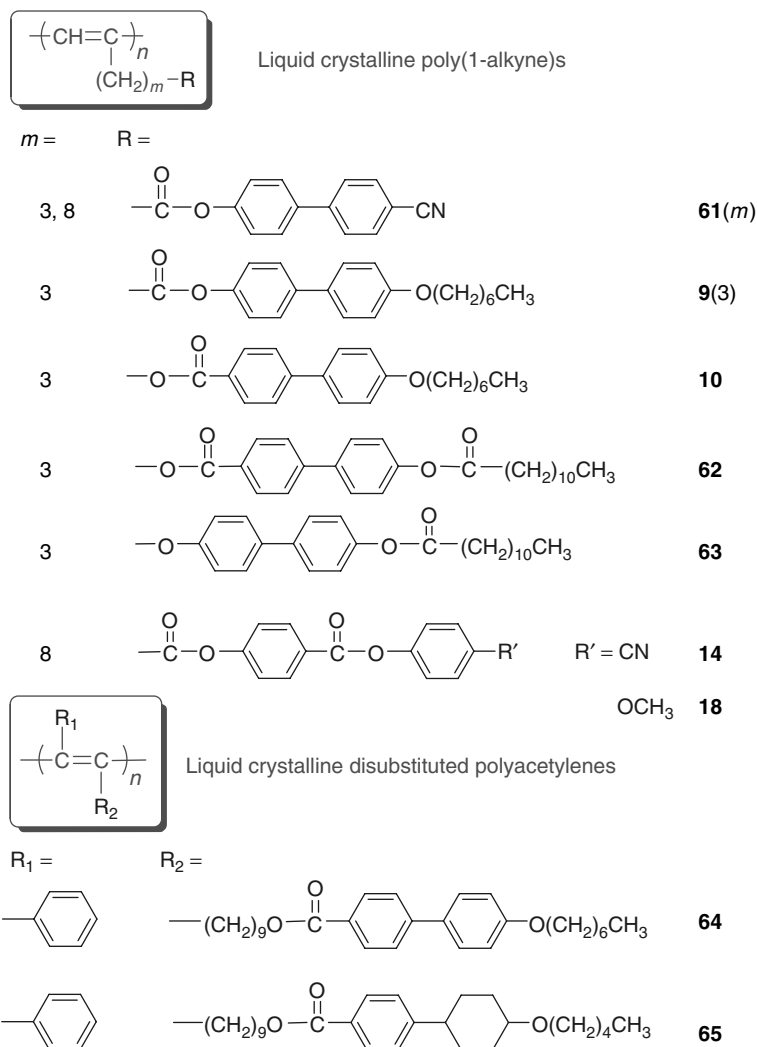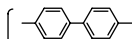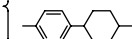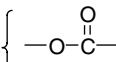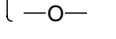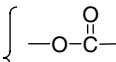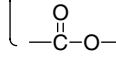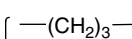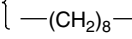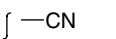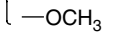
Chart 1.7 Examples of liquid-crystalline PAs.

The elemental composition or molecular formulae for **9**(3) and **10** are exactly the same; the two polymers differ only in the orientation of their ester bridge. This small difference changes the mesogenic packing: the mesostructure of **10** involves mixed monolayer and bilayer packing arrangements, whereas the mesophase of **9**(3) is associated with a pure bilayer mesogenic alignment. An increase in the length of the flexible spacer encourages better mesogenic order and induces a transition from nematicity to smecticity in the poly(1-alkyne)-based system **61**(*m*) (Table 1.1, nos. 7 and 8). The increase in the spacer length also widens the LC temperature range (ΔT); in the case of **61**(*m*), ΔT for **61**(8) is approximately three

Table 1.1 Effects of molecular structures on the mesogenic packing of liquid-crystalline PAs[a].

No.	Structural variation		Mesophase	$T_c - T_m$(°C)	ΔT(°C)
1	Mesogenic core	64	S_A	172−158	14
2		65	N	108−90	18
3	Functional bridge	62	S_{Ad}	199−162	37
4		63	S_A	180−122	58
5	Bridge orientation	10	$S_A + S_{Ad}$[b]	174−100	74
6		9(3)	S_{Ad}	206−127	79
7	Flexible spacer[c]	$-(CH_2)_3-$ 61(3)	N	189−152	37
8		$-(CH_2)_8-$ 61(8)	S_{Ad}	190−81	109
9	Functional tail	$-CN$ 14	S_A	195−80	115
10		$-OCH_3$ 18	S_A-N[d]	141−114−96	45

[a]Data taken from the DSC thermograms recorded under nitrogen in the first cooling scan.
[b]Coexistent mono- (S_A) and bilayer (S_{Ad}) mesophases.
[c]For mesogenic poly(1-alkyne)s.
[d]Consecutive S_A and N mesophase transitions.
  Abbreviations: S_A, Smectic A phase; N, nematic phase; S_{Ad}, interdigitated smectic A phase; T_c, clearing point; T_m, melting point; ΔT, $T_c - T_m$ (temperature range of the liquid-crystalline phase).

times higher than that for **61**(3). The polymer with polar cyano tails (**14**) undergoes an enantiotropic S_A transition over a wide temperature range (115 °C), but its counterpart with less polar methoxy tails (**18**) goes through enantiotropic S_A and N transitions in a narrow temperature range (Table 1.1, nos. 9 and 10).

The most distinct structural feature of the LCPAs is the rigidity of their double-bond backbones, in comparison to the flexibility of the single-bond backbones of nonconjugated polymers. According to the researchers of LC polymers, a stiff backbone is generally regarded as a structural defect that distorts the packing arrangements of mesogens, which is why the flexible backbones of polysiloxane and polyacrylate, for example, have often been used in the design and synthesis of "conventional" LC polymers. Is a rigid backbone only destructive or can it play any constructive role? It is envisioned that an oriented rigid main chain might induce unique alignments of its mesogenic side chains. The stiff backbone of an LCPA possesses a long relaxation time, and a mechanically oriented LCPA system

(a)   (b)
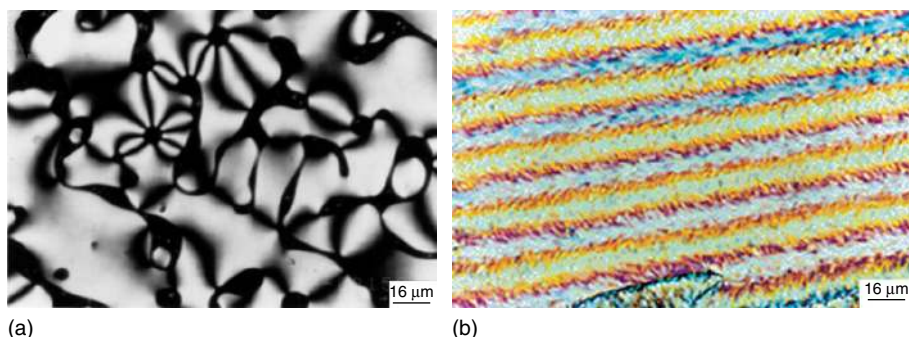
Figure 1.5 (a) Schlieren textures with disclination strengths of 3/2 and 2 observed after a rotationally agitated **18** has been annealed at 136 °C for 5 minutes. (b) Induced alignments of **18** by mechanical shear.

may not quickly return to the preperturbed state, thus offering the opportunity to generate macroscopic anisotropy by the application of a mechanical force.
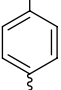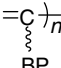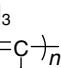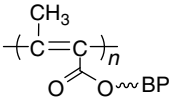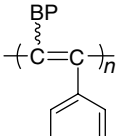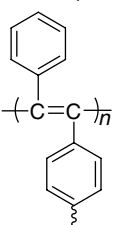
To examine its response to mechanical perturbation, a rotational force was applied to **18** when it was cooled from the isotropic state to the N phase. Interestingly, unusual high-strength disclination strengths of 3/2 and 2 are observed (Figure 1.5a) [37], which have been found in a few systems of main-chain LC polymers with rigid backbones but never in any systems of side chain LC polymers with flexible backbones. The high disclination values are demonstrative of the backbone rigidity of the LCPA, because only a stiff backbone can survive the severe director field distortions involved in the formation of the high-strength disclinations. When a shear force is applied to the N phase of **18** at ∼140 °C, inversion walls are generated. Natural cooling of the system to room temperature results in the formation of well-ordered parallel microbands (Figure 1.5b) [37]. In general, a main-chain LC polymer with a rigid backbone can be easily aligned by a shear force, while a side chain LC polymer with a flexible backbone can be readily processed by solution processes. Evidently, **18** possesses the combined advantages of main- and side chain LC polymers: it can be readily aligned by a shear force and can in the meanwhile be easily processed because of its excellent solubility in common organic solvents.

1.3.3
Luminescence

The study of luminescence properties of π-conjugated polymers is a hot topic of great current interest. Whereas PA is an archetypal π-conjugated polymer, little work had been done on the development of light-emitting polyacetylenes (LEPAs) in the early time, because PA itself is a very poor luminophore. Modifications of molecular structure of PA, such as attachments of the pendant groups with different electronic and steric effects, have been used to tune the conjugation length along

Table 1.2 Photoluminescence of PAs bearing biphenyl (BP) pendant.

No.	Polymer	Skeleton	Emitting center	Emission color	Quantum yield
1	PA	$+CH=CH +_n$	Backbone	IR	Low
2	PPAs	$+HC=C +_n$ BP	Pendant	UV	Low
3	Poly(1-alkyne)s	$+HC=C +_n$ BP	Pendant	UV	Medium
4	Poly(propiolate)s	$+C=C +_n$ CH₃ O O ~~~BP	Pendant	UV	High
5	Poly(1-phenyl-1-alkyne)s	BP $+C=C +_n$	Skeleton	Blue	High
6	Poly(diphenylacetylene)s	$+C=C +_n$ BP	Skeleton	Green	High

the polyene backbone and the electronic interaction between the polymer chains. These approaches have worked well and led to the generation of a large variety of LEPAs with high photoluminescence (PL) and good electroluminescence (EL) efficiencies. In the LEPAs, the emitting center can be pendant or backbone, the energy transfer can be from pendant to backbone or from backbone to pendant, and the emission color can be violet, blue, green, or red – all tunable by changing the backbone and pendant structures.

A typical example is the study of the PL performances of PAs bearing a BP pendant, as shown in Table 1.2 [1, 2, 23, 33, 34, 39–42]. The data for the parent form of (unsubstituted) PA are also given in the table for the purpose of comparison; it emits very weakly in the infrared spectral region due to the existence of exciton

traps in the polyene backbone. Similarly, PPA itself is a poor light emitter owing to the photogenerated radical defects in the conjugated skeleton. The PPA derivative with BP pendant emits UV light with a low Φ_F value, because the light emitted from the BP pendant is partially quenched by the defects in the PPA skeleton (Table 1.2, no. 2). When the PPA skeleton is changed to a poly(1-alkyne) one, the Φ_F value is increased due to the alleviated quenching by the poly(1-alkyne) skeleton. Disubstituted poly(propiolate)s, however, luminesce efficiently (Table 1.2, no. 4), because of their photochemically stable, defect-free skeleton structure.

From the result of disubstituted poly(propiolate)s, it is envisioned that if the hydrogen atom in the repeat unit of a poly(1-alkyne) is replaced by a bulky aromatic substituent, the backbone would become twisted and more stable. The steric effect would shorten the effective conjugation length of the resultant disubstituted PAs, hence widening their bandgap and shifting their skeleton emission from IR to visible. Indeed, poly(1-phenyl-1-alkyne)s emit strongly in the blue region (Table 1.2, no. 5). Meanwhile, the polymer skeleton absorbs the UV light emitted from the BP pendant, which helps enhance the light emission efficiency. Following this strategy, BP-containing poly(diphenylacetylene) derivatives have been synthesized, whose emission efficiencies are comparably high but their emission colors are redshifted to green.

The molecular engineering endeavors change not only the location of the emitting center, as discussed above (Table 1.2), but also the direction of the energy transfer, as exemplified in Chart 1.8 [41, 42]. In polymer **21**, an efficient fluorescence energy transfer (FRET) process occurs from the green light-emitting silole pendant to the red light-emitting polyene backbone, because of the direct electronic communication between the pendant and the backbone. The PA backbone of **21** emits faintly in the long-wavelength region, in agreement with the early observation that pure PA is a weak IR emitter. In polymer **34**, however, the FRET is from the poly(1-phenyl-1-alkyne) skeleton to the silole pendant. The blue light emitted from the skeleton excites the pendant, resulting in the emission of green light. Polymer **35** emits green light efficiently, because the excited states of the silole pendant and the poly(diphenylacetylene) skeleton both undergo radiative transitions in a similar spectral region.

Aggregation of conjugated polymer chains in the solid state often results in the formation of less-emissive or nonemissive species, such as excimers and exciplexes, which partially or completely quench the luminescence of the polymers. This aggregation-caused quenching effect has been a thorny problem in the development of efficient polymer light-emitting diodes (PLEDs), because the conjugated polymers are commonly used as thin solid films in the EL devices

During our search for efficient light-emitting materials, we found a group of highly luminescent organometallic molecules called *siloles in the solid state*. They exhibit an invaluable effect of aggregation-induced emission (AIE) [43]: they are practically nonluminescent when molecularly dissolved in solution but become strongly emissive when aggregated in poor solvents or fabricated into solid films. 1,1,2,3,4,5-Hexaphenylsilole (HPS) is a typical paradigm of AIE luminogen
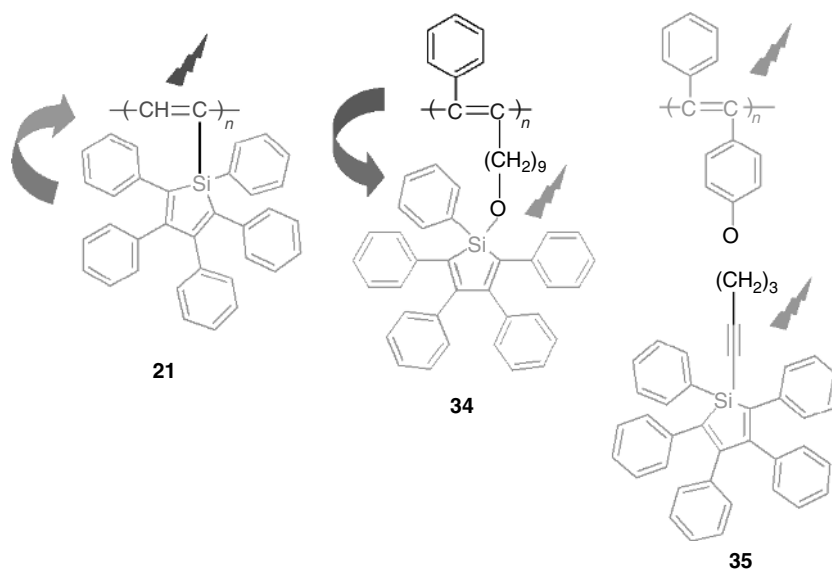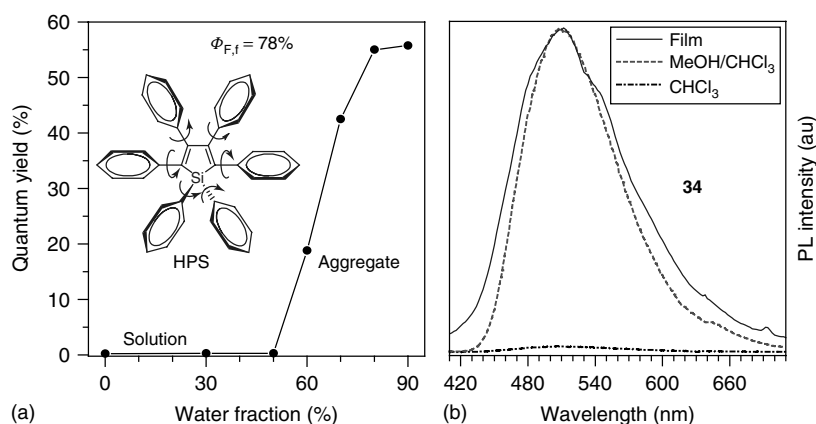
Chart 1.8 Energy transfers in luminescent PAs.

Figure 1.6 (a) Quantum yield (Φ_F) of HPS versus composition of acetonitrile/water mixture. The quantum yield of its film ($\Phi_{F,f}$) is shown for comparison. (b) Photoluminescence spectra of **34** in chloroform (molecularly dissolved solution), a methanol/chloroform mixture (9 : 1 by volume; nanoaggregate suspension), and solid state (thin film).

(Figure 1.6a). Its Φ_F value in pure acetonitrile is as low as 0.2%. The Φ_F almost remains unchanged when up to 50% of water is added into the acetonitrile solution but starts to swiftly increase afterward due to the formation of nanoaggregates. When the water content is 90 vol%, the Φ_F rises to ~56%, which is ~280 times higher than that in the acetonitrile solution [44]. In the film state, the Φ_F is

even higher and goes to ∼78% [45]. Through experimental and theoretical studies [46, 47], the AIE mechanism can be understood as follows. In the dilute solution at room temperature, the active intramolecular rotations of the peripheral phenyl rings of HPS around the axes of the single bonds linked to the central silole core nonradiatively annihilate the excitons, thereby making the silole molecules nonemissive. In the aggregates, the propeller shape of the silole molecules prevents them from forming excimeric species but the physical constraint in the solid state restricts their intramolecular rotations, which blocks the nonradiative relaxation channels and populates the radiative decay, thus making the silole molecules luminescent.

Siloles are thus a group of excellent molecules for LED applications [44, 48]. Low MW compounds, however, have to be fabricated into thin films by relatively expensive techniques such as vacuum sublimation and vapor deposition, which are not well suited to the manufacture of large-area devices. One way to overcome this processing disadvantage is to make high-MW polymers, which can be readily processed from their solutions into thin solid films over large areas by simple spin coating or doctor's blade techniques. Motivated by these considerations, we incorporated the silole moiety into the poly(1-phenyl-1-alkyne) as a pendant, with the aim of generating AIE-active polymers. HPS-containing poly(1-phenyl-1-alkyne) **34** is an example of such polymers. The solution of **34** is virtually nonluminescent (Figure 1.6b) [41], because in the FRET process of this polymer, the PL from the emissive poly(1-phenyl-1-alkyne) skeleton is quenched by the nonemissive HPS pendant. Thanks to its AIE attribute, the Φ_F value of its nanoaggregates in the methanol/chloroform mixture with 90% methanol is ∼46-fold higher than that in the chloroform solution.

Retrostructural analysis of another AIE-active 1,1,2,2-tetraphenylethene (TPE) developed by us reveals that there is one common structural feature between TPE, and disubstituted poly(1-phenyl-1-octyne) **66** and poly(diphenylacetylene) **67**: one or more aromatic peripheries are connected to an olefinic core [49–53]. In a dilute solution of TPE, intramolecular rotations of the aromatic rings against the olefinic core effectively and nonradiatively deactivate the excited states, thus making the molecules nonemissive ("off"). In the aggregate state, such rotations are restricted. The blockage of the nonradiative decay channels turns the light emissions "on." Therefore, it is expected that **66** and **67** shown in Chart 1.9 might show an aggregation-induced emission enhancement (AIEE) effect, since the polymers themselves are already emissive in solution. As anticipated, **66** and **67** are AIEE active, in which the emission intensities are progressively increased with the increasing water fraction in the THF/water mixture (Figure 1.7) [54, 55]. Spectral profile of **66** remains unchanged [54], while the emission spectrum of **67** gradually redshifts [55].

Further studies of the light-emitting behaviors of these disubstituted PAs reveal that their PL spectra are commonly very broad and lack of fine structures, characteristic of excimer emissions. According to the "$n = 3$ rule" shown in Chart 1.10, molecules with phenyl rings spatially separated by three carbon atoms (e.g., 1,3-diphenylpropane and PS) [56, 57] can form intramolecular excimers
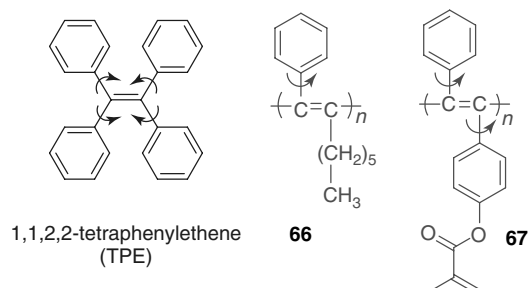
1,1,2,2-tetraphenylethene
(TPE)   **66**   **67**

Chart 1.9 Intramolecular rotations in TPE and disubstituted PAs.
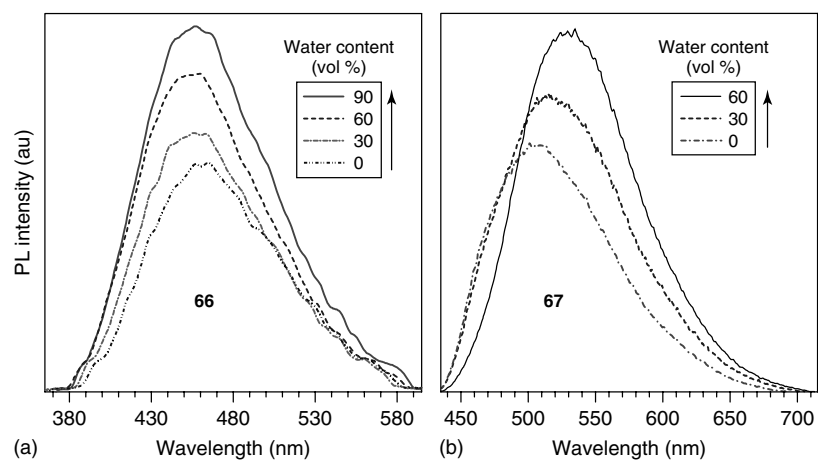
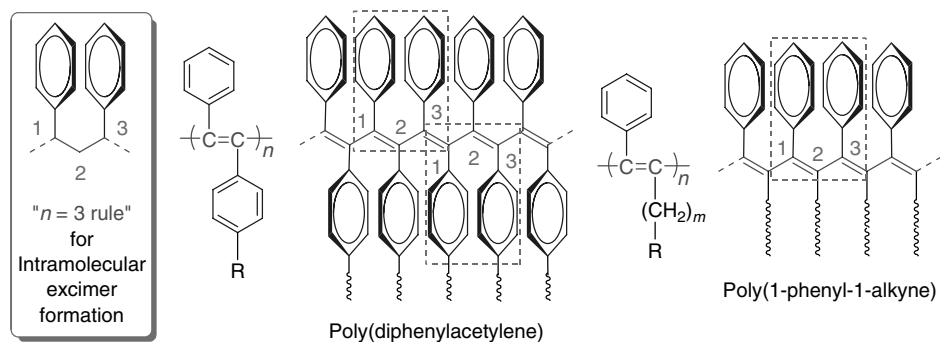**Figure 1.7** Photoluminescence spectra of (a) **66** and (b) **67** in THF/water mixtures.

"$n = 3$ rule"
for
Intramolecular
excimer
formation

Poly(diphenylacetylene)

Poly(1-phenyl-1-alkyne)

Chart 1.10 Formation of intramolecular excimers in disubstituted PAs.

that emit in the redder spectral regions, in comparison to their ''monomer'' emissions [54, 55]. Both the poly(diphenylacetylene) and poly(1-phenyl-1-alkyne) derivatives follow this ''$n = 3$ rule.'' In general, this rule has been used to explain why light emissions of organic dyes are quenched in the aggregate state, while we have, however, found that the poly(diphenylacetylene) and poly(1-phenyl-1-alkyne) derivatives show an ''abnormal'' AIEE phenomenon: their light emissions are enhanced by aggregate formation.

Through the systematic investigations assisted by theoretical calculations, we have gained some insights into the relationship between the AIEE effect and the intramolecular excimer formation. In the poly(diphenylacetylene) and poly(1-phenyl-1-alkyne) skeletons, some ''$n = 3$'' intramolecular or intrachain excimer pairs have already formed in the solution state, as indicated by the broad and structureless spectra of the polymer solutions, although because of the polyene backbone twisting, the phenyl ring pairing is disrupted at some places, leaving some phenyl rings unpaired and standing alone as monomers. Upon formation by aggregration, the volume shrinkage of the poly(diphenylacetylene) chains in the solvent mixture with poor solvating power puts the phenyl rings in closer vicinities. This enhances the $\pi-\pi$ stacking interactions of the phenyl rings and restricts their intramolecular rotations: the former effect populates the excimer species, hence redshifting the emission spectrum, while the latter effect boosts its emission intensity, hence the observed AIEE phenomenon. In the poly(1-phenyl-1-alkyne) system, however, the population of the excimers does not change too much with aggregate formation, hence no apparent redshift in the PL spectrum. A unique feature to be noted in this system is that the twisted polyene backbone and long side chains weaken the interactions between the polymer strands, which helps prevent the light emission of polymer from being quenched by the formation of interchain excimers.

The LEPAs enjoy good spectral stability: for example, **32**(4) emits a blue light, whose PL profile does not vary after it has been heated to 200 °C in air or exposed to UV irradiation under nitrogen or under vacuum (Figure 1.8a) [58]. The efficient PL encouraged us to check EL of the LEPAs. The PLED of **32**(4) emits a blue light of 460 nm, whose EL peak is symmetrically shaped with no sideband. Its external quantum efficiency (η_{EL}) reaches 0.85%, comparable to those of some of the best blue light-emitting polymers. Although the device configurations of our PLEDs have not been optimized, many of them already display an η_{EL} of 0.5–0.86%, much higher than that (0.01%) of nonfunctional poly(1-phenyl-1-octyne) (**66**). Polyfluorenes are the best-known blue light-emitting polymers, but their spectral stabilities are low. A broad peak centered at ∼520 nm appears when a current density as low as 1.8 mA cm^{-2} passes through the poly(9,9-dioctylfluorene) (PDOF) device (Figure 1.8b). The EL spectrum of **32**(4) does not change when a current density as high as 127 mA cm^{-2} passes through its device. This demonstrates that disubstituted PAs are thus spectrally very stable.
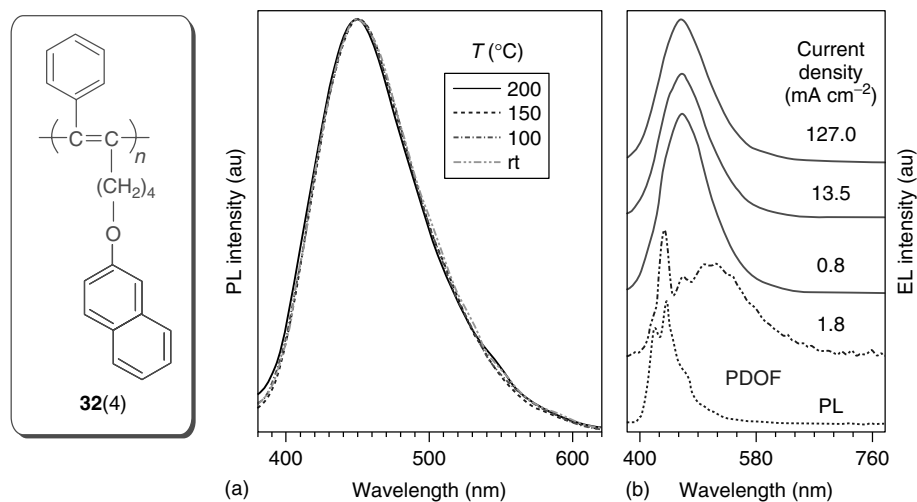
Figure 1.8 (a) Spectral stability of **32**(4) against thermolysis. (b) Comparison of its EL spectral stability with that of poly(9,9-dioctylfluorene) (PDOF).

1.3.4
Fluorescence Sensing

Fluorescent conjugated acetylenic polymers have been actively used for fluorescent sensors by virtue of their specific PL responses to interactions with analytes. PL of some LEPAs can make different responses to different metal ions. For example, when one equivalent of Cu^{2+} ion is added to a solution of **37a**, its PL drops to half the original value(Figure 1.9) [21]. The effect of Fe^{3+} is more striking: it completely quenches the emission. In contrast, the PL becomes stronger in the presence of Al^{3+}. These distinct PL responses associated with the specific polymer–metal interactions enable the LEPA to act as a chemosensor.

We developed a sequential chemosensor based on imidazole-containing LEPA **68** (Scheme 1.7). Among the different kinds of metal ions, only Cu^{2+} ion can completely and efficiently quench or turn off the strong fluorescence of **68**, with a detection limit as low as 1.48 ppm [20]. The associated Stern–Volmer quenching constant (K_{sv}) is as high as 3.7×10^5 M^{-1}, because of the high affinity of Cu^{2+} ion toward imidazole group, which enables the polymer to differentiate Cu^{2+} from other metallic ions. The Cu^{2+}-quenched light emission of **68** can be turned on by the addition of CN^- ion, thus allowing the polymer to function as a unique dual-response sequential ionosensor for cyanide detection.

1.3.5
Patterning and Imaging

If a processable polymer enjoys both photosensitive and light-emitting properties, it will be an excellent photoresist candidate for the fabrication of a luminescent
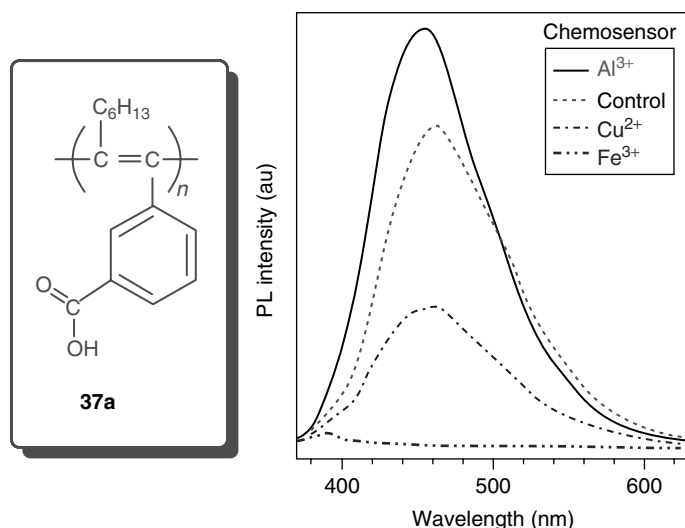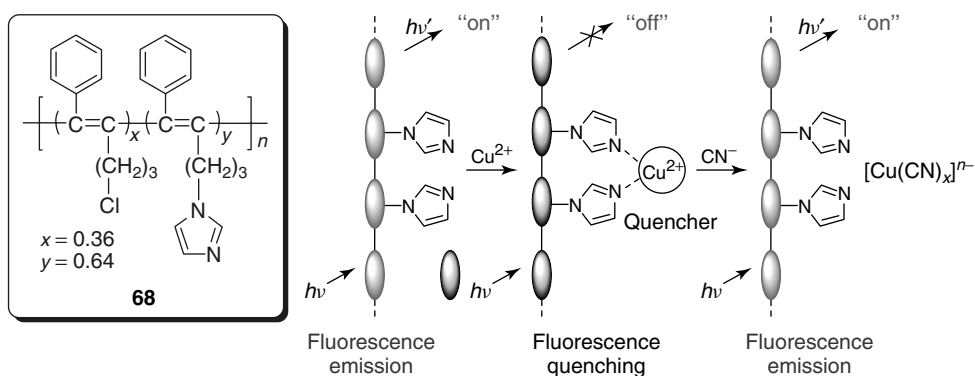
Figure 1.9 Tuning photoluminescence of THF solutions of **37a** by ionic species.

Scheme 1.7 Sensing Cu^{2+} and CN^- ions by an imidazole-functionalized PA.

pattern by the photolithography technique. Given this reason, many LEPAs fulfill the requirements and are thus promising photoresist materials for applications in photonic and electronic devices, and biological sensing and probing chips (e.g., LEDs, liquid crystal display, and medicinal diagnostic biochip).

UV irradiation of **69** readily initiates photo-polymerization of its acrylic pendants (Figure 1.10a) [55]. Development of the exposed films gives well-defined photoresist patterns (Figure 1.10c,d). The patterned lines glow under UV illumination, because its poly(diphenylacetylene) skeleton is highly emissive in a green color. Disubstituted PAs are resistant to thermolysis. Some of them, however, are sensitive to photo-oxidation, which quenches their PL. For example, UV irradiation of a film of **20**(4) in air through a mask quenches the luminescence of the exposed region
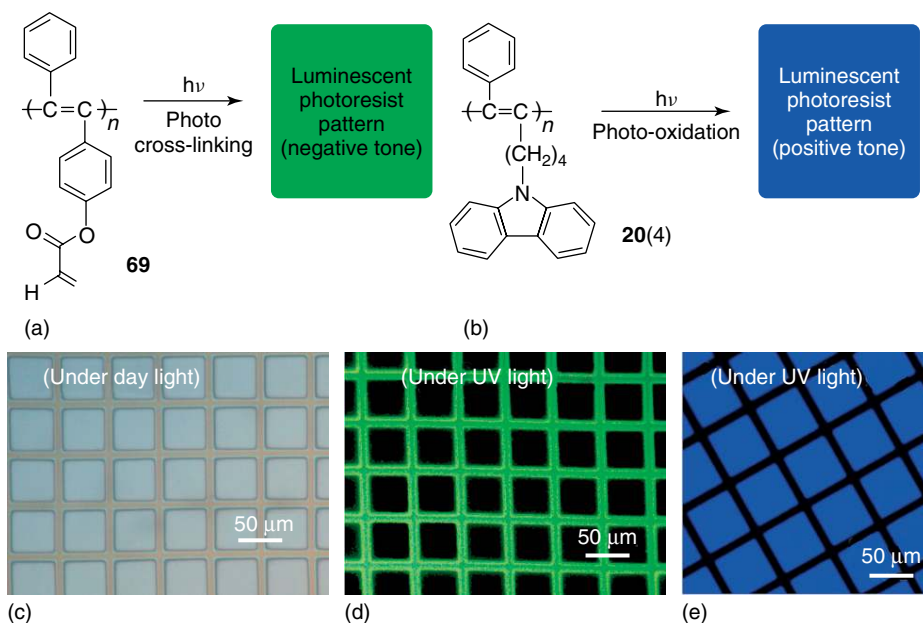
Figure 1.10 (a) Photo-cross-linking of **69** and (b) photo-oxidation of **20**(4) lead to the formation of (c and d) negative and (e) positive photoresist images.

(black lines) (Figure 1.10e), while the exposed area remains emissive in a blue color [59]. A PL image is thus directly drawn without a developing process.

1.3.6
Chromism

The polyene backbone of a segment in a PA chain can adopt *E-s-E, E-s-Z, Z-s-E,* or *Z-s-Z* conformation [4, 10, 34]. Because the energy needed for the conformational conversion is small, the conformation of a PA segment is anticipated to be tunable by changing its surrounding environment. In toluene and chloroform, **28e** absorbs weakly and strongly, respectively (Figure 1.11a). The optical transition between these two states can be manipulated continuously and reversibly by varying the ratio of the solvents in the polymer solution. Most segments of **28e** may adopt a more planar conformation in chloroform while the opposite is true in toluene, thereby accounting for the solvatochromism.

The light transmission spectrum of **19** resembles that of an optical cutoff filter, which redshifts with an increase in its concentration (c) (Figure 1.11b). Its cutoff wavelength (λ_c) changes semilogarithmically with c over a wide spectral range [60], which is possibly due to nanocluster formation. This offers an easy way to make a plastic optical filter, whose λ_c can be readily tuned by varying its PA content.
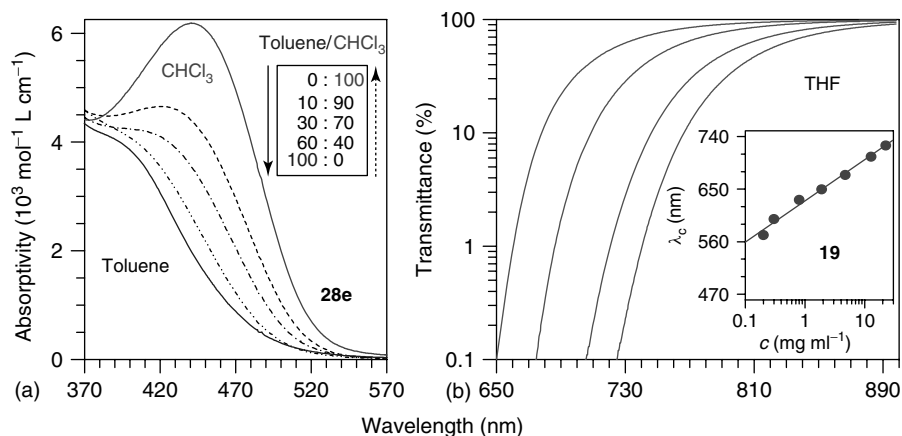
Figure 1.11 (a) Solvato- and (b) concentratochromisms of **28e** and **19**.

1.3.7
Optical Activity

Tang synthesized one of the few optically active polyacetylenes (OAPAs) in the late 1980s [61]. He continued his pursuit of OAPAs after he had moved to Hong Kong in the mid-1990s. While the early OAPAs contained no polar groups owing to the difficulty of synthesizing them, the recent advancements in the polymer syntheses allow us to design a diverse palette of new OAPAs by incorporating various chiral units into the PA chains.

We have concentrated our efforts on the development of OAPAs with naturally occurring building blocks such as amino acids, saccharides, nucleosides, and sterols [62–73]. Figure 1.12a shows circular dichroism spectra of a pair of polymers containing D-[**22e**(D)] and L-α-phenylglycine units [**22e**(L)]. The positive and negative Cotton effects in the long-wavelength region reveal that the chain segments of the PAs carrying the pendants of opposite chirality form spirals of opposite helicity. Obviously, the backbone helicity (M/P) is determined by the pendant chirality (D/L) under the same environmental conditions. When solvent of the polymer solution is changed from chloroform to THF, the Cotton effect is greatly decreased, indicating that the helical preference of the chain segment can be tuned by an environmental variation. The helical chain segments are believed to be mainly stabilized by the intra- and interstrand hydrogen bonds between the chiral pendants (Figure 1.12b,c). The noncovalent stabilization can be broken by external perturbation and the system will reach a new equilibrium. This dynamic process enables the OAPAs to cope with the variations in their surrounding environments, as do helical biopolymers such as proteins.

Further examples of the helicity tuning by external stimuli are given in Figure 1.13 [68]. The ellipticities ([θ]) of **23e** are positive and negative in THF and CHCl$_3$, respectively; that is, the majority of its chain segments form coils of opposite helicity

(a)

(b) Intrachain H-bonding

(c) Interchain H-bonding
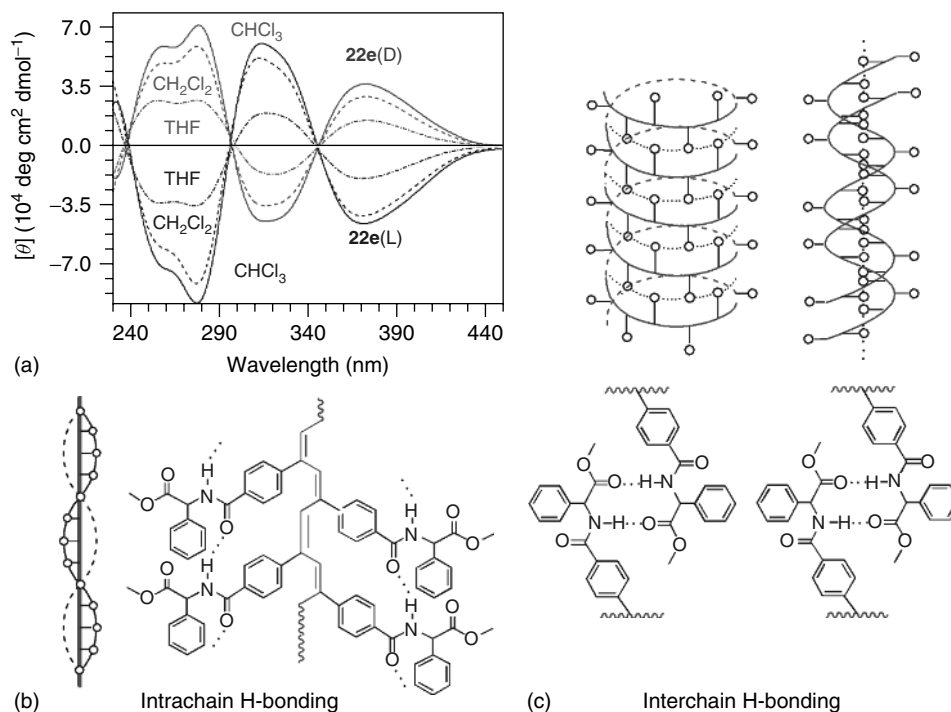
Figure 1.12 (a) Chain helicity determined by pendant chirality and manipulated by solvent variation. (b) Single and (c) double helical strands of **22e** stabilized by intra- and interchain hydrogen bonds.

in these two solvents. In other words, the helical preference can be completely reversed by simply changing the solvent. The helicity change is continuous and reversible, as revealed by the $[\theta]$–solvent plot in Figure 1.13a. Ellipticity changes rapidly when the amount of chloroform is increased from ∼65 to ∼80%. This is indicative of a cooperative process: once some segments are associated via noncovalent interactions (e.g., hydrogen bond), their neighboring segments will be zipped up quickly along the preferred direction. The ellipticity of **23e** monotonically decreases with increasing temperature because the thermally activated chain randomization induces the segments to unwind.

Addition of KOH to a solution of **23a** progressively weakens its $[\theta]$, because the ionic interaction of K^+ with CO_2^- breaks the intra- and interchain hydrogen bonds (Figure 1.13c) [64]. The original $[\theta]$ can be regained when the KOH solution is neutralized by HCl; this illustrates the reversibility of helicity tuning with variation in the pH. Intriguingly, $[\theta]$ can also be tuned by achiral additives. With continuous addition of glycine (an achiral essential amino acid) to the solution of **23a**, its $[\theta]$ also continuously increases. The glycine molecules may bind to the ʟ-valine pendants, causing an increase in the pendant bulkiness and thereby inducing further twists in the chain segments.
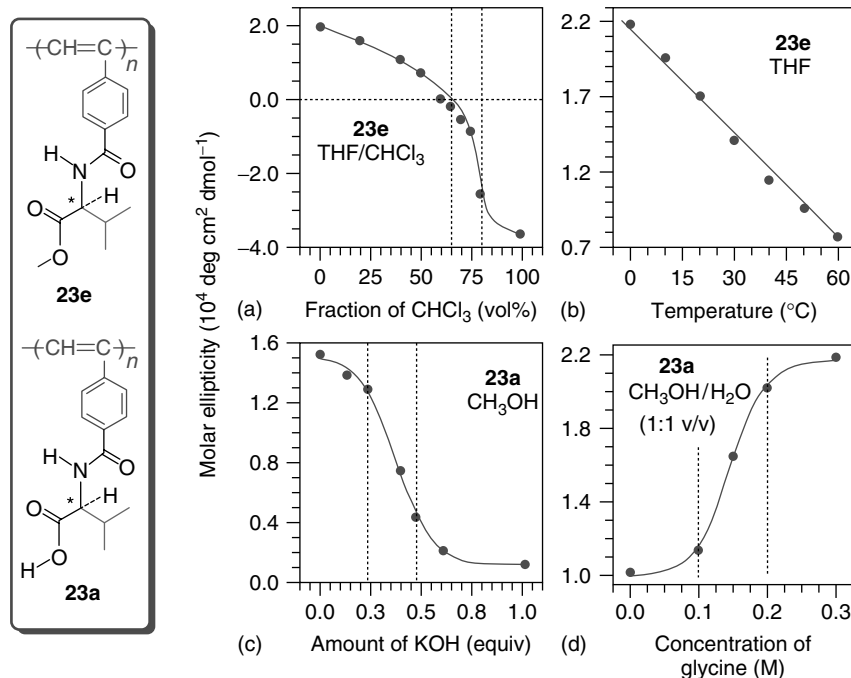
Figure 1.13 Tuning ellipticity of **23e** (a,b) and **23a** (c,d) at ∼375 nm by (a) solvent, (b) temperature, (c) pH, and (d) additive.

1.3.8
Supramolecular Assembly

After studying the chain helicity as associated with the secondary structure of the OAPAs, we investigated their higher-order structures. Noticing the unique amphiphilicity of the OAPAs originating from their hydrophobic backbones and hydrophilic pendants, we explored the possibility of utilizing them as ''Legos'' to construct biomimetic hierarchical structures.

The OAPAs can self-organize into a variety of morphologies reminiscent of natural structural motifs such as vesicles, tubules, helixes, and honeycombs. Thus, evaporation of a solution of **30e** (an OAPA with uridine pendants) yields vesicles, whilst that of **24a** (L-isoleucine pendants) gives tubules with coexisting vesicles (Figure 1.14) [62]. In the polar solvents, the OAPAs cluster into bi- or multilayered spherical aggregates or vesicles with hydrophobic cores and hydrophilic coronas. Under appropriate conditions, the vesicles further associate into the tubular structures.

The tunability of chain helicity of the OAPAs through internal and external perturbations suggests that their self-assembling morphologies can be manipulated by changing their molecular structures and environmental conditions, because the
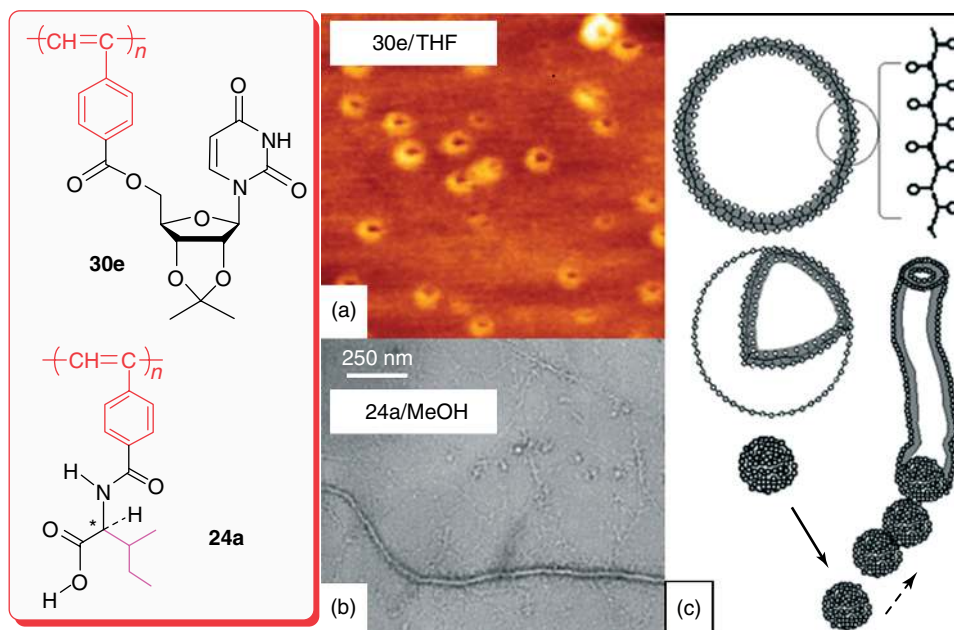
Figure 1.14 (a) Vesicles and (b) nanotubes formed by natural evaporation of PA solutions (10–19 μM), and (c) proposed processes for the formation of the nanostructures.

variations in the secondary structure should affect the higher-order structures. This proves to be the case. Evaporation of a methanol solution of **23e** gives a string of pearls (Figure 1.15a). Helical ropes are obtained when its structure (internal) and solvent (external) are changed to **23a** and THF, respectively (Figure 1.15b,c). Addition of KOH to the methanol solution of **23a** changes the helical cable to random thread (Figure 1.15d). The association of K^+ ions with CO_{2^-} groups breaks the hydrogen bonds. The charged polyelectrolyte chains repulse each other and are difficult to associate into multistrand helical cables, hence the observed thin random coils [64].

Evaporation of more concentrated solutions gives structures of bigger sizes: for example, a large honeycomb pattern is obtained from a thick solution of **25a** (Figure 1.16a) [74]. Precipitation of a concentrated solution of **26e** into its poor solvents yields micron-size helical fibers with both left- and right-handed twists (Figure 1.16b) [75].

1.3.9
Optical Nonlinearity

Conjugated organic materials exhibiting strong NLO properties and fast response time have attracted considerable interest because of their potential high-tech
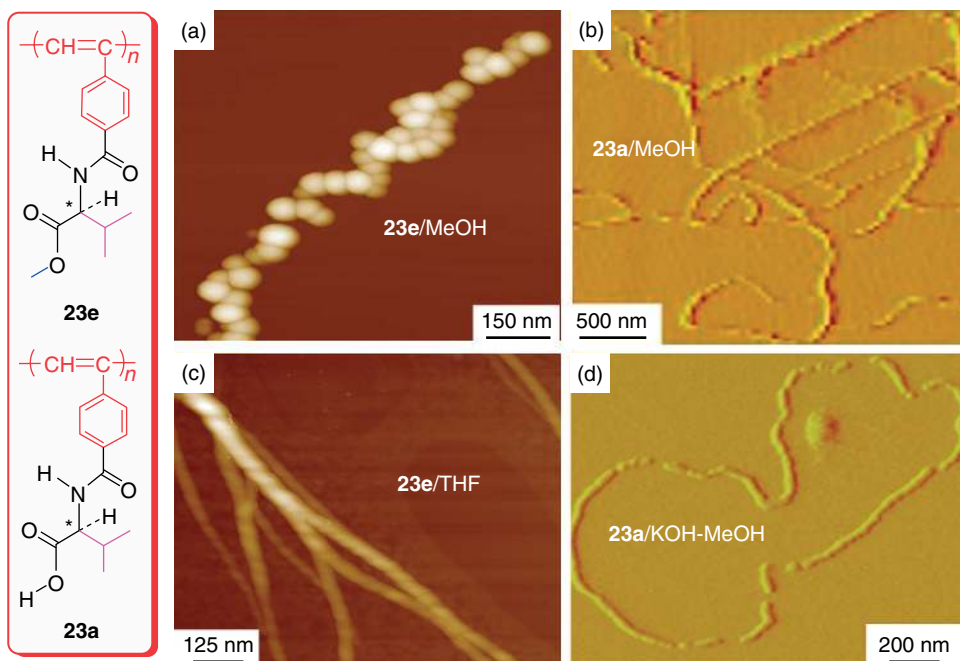
Figure 1.15 Tuning the assembling structures formed by natural evaporation of the solutions of **23(a,c)** and **23(b,d)** ($\sim 11.6-12.2$ µM) through internal and external perturbations.

applications in various optical and photonic devices. Of particular interest is the optical limiter, which is a novel optical material that transmits light of normal intensity but attenuates light of high power. In other words, it allows mild light to pass through but prevents harsh light from being transmitted. The rapid advancements in the laser-based technologies and the growing enthusiasm in the Space exploration have motivated intensive research efforts in the development of new optical limiting materials with novel structures and improved performances.

Substituted PAs with various functional groups have been found to enjoy excellent optical limiting and NLO properties. Many research groups have studied their third-order NLO properties derived from their π-conjugated nature. Azobenzene is a well-known second-order NLO-active chromophore. Incorporating such a chromophore into PAs might offer materials with novel optical properties. We synthesized a series of PAs with NLO properties [76–80]. Figure 1.17 shows the optical limiting properties of the polymers **70** and **71** with azobenzene as the pendant at the same linear transmittance ($T = 75\%$) [76]. All the polymers are good optical limiters, especially for those with short spacer lengths. For example, the limiting threshold and limiting amplitude of **70**(3) are 0.245 and 0.349 J cm^{-2}, respectively, which are 1.3 and 1.2 times lower than those of **70**(8). The optical limiting properties are also affected by the ring substituent: the polymer
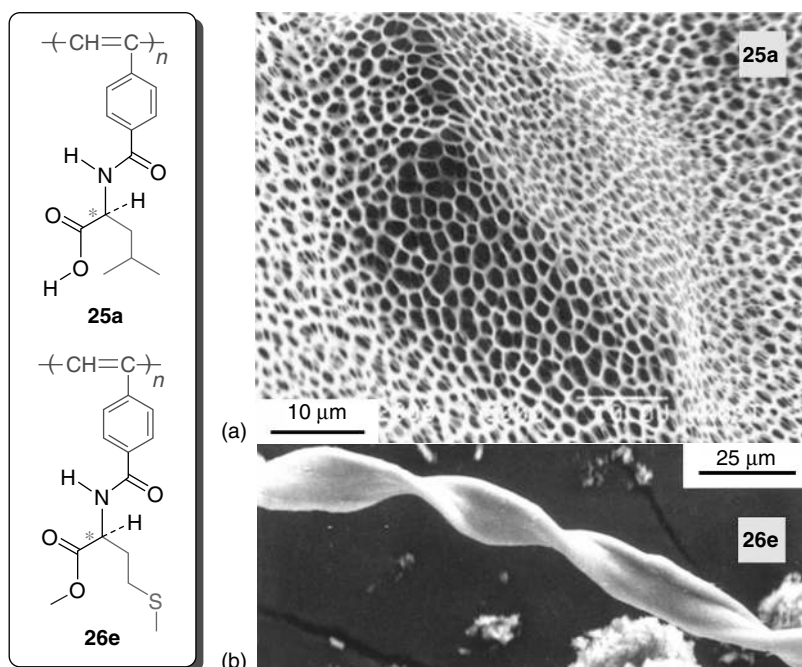
Figure 1.16 (a) Honeycomb pattern and (b) helical fiber formed by (a) evaporation of **25a**/MeOH solution (29 μM) on glass slide and (b) precipitation of **26e**/DMF solution (100 mM) into acetone/ether mixture.

containing bromo substituent shows inferior performance, as understood from the comparison of the limiting threshold (0.295 J cm^{-2}) and saturation fluence (0.393 J cm^{-2}) of **71**(3) with those of **70**(3).

Fullerenes are known to limit intense optical pulses via a reverse saturable absorption mechanism. The fullerene tips and the graphene sheets of the CNTs also undergo NLO absorption processes, while their cylindrical bodies, although with high aspect ratios, are light-scattering centers. Both the NLO absorption and the light scattering make the CNTs promising for optical limiting applications. C$_{60}$ and CNTs, however, have notoriously poor solubility and processability. Hybridization of C$_{60}$ and CNTs with processable π-conjugated polymers is a promising way to enhance the solubility of the carbon allotropes, with the possibility of generating new materials with novel properties. Our group has done a pioneering work in wrapping CNTs with conjugated polymers. In 1999, our group successfully prepared PPA/CNT nanohybrid by *in situ* polymerization technique [81], and thereafter established a platform to prepare a series of PA/CNT and PA/C$_{60}$ nanohybrids by physical and chemical methods as shown in Scheme 1.8 [82, 83].

The optical limiting performances of PPA/CNT and **72**/C$_{60}$ nanohybrids are shown in Figure 1.18 as examples. The data for the parent forms, that is, PPA and C$_{60}$, are given in the same figure for comparison [81, 83]. When a THF
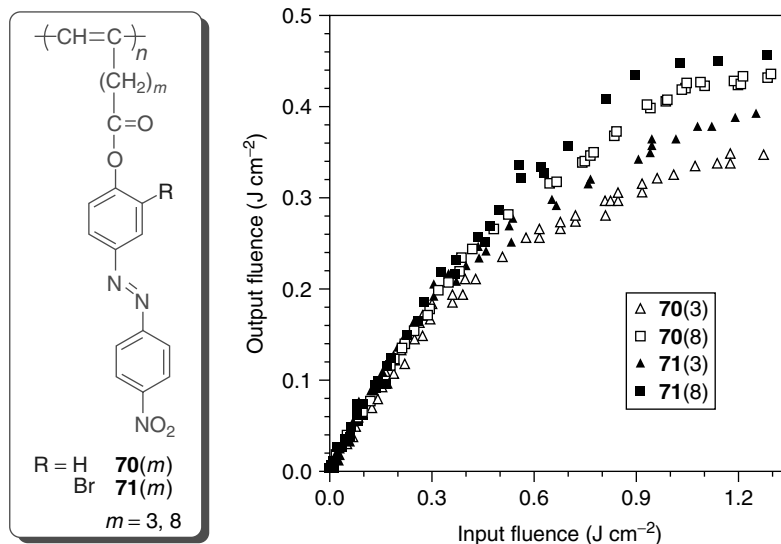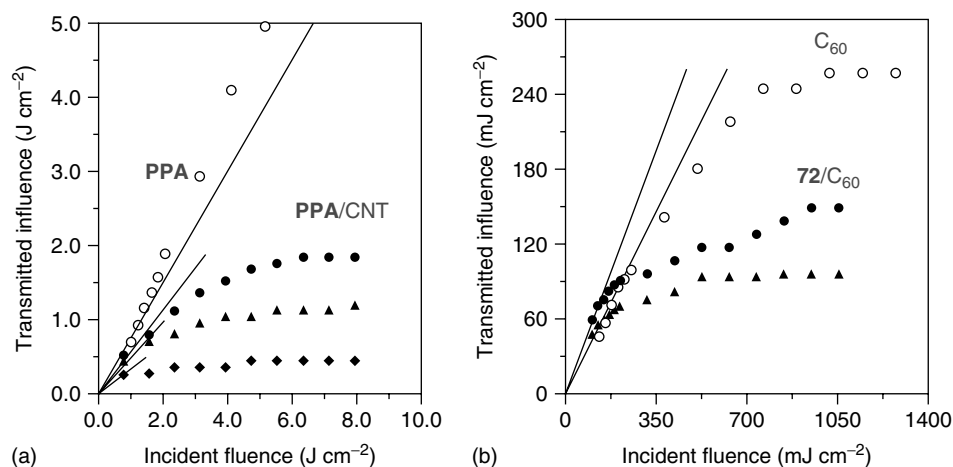
Figure 1.17 Optical limiting responses to 8-ns, 532-nm laser light, of THF solutions of **70**(*m*) and **71**(*m*) with a linear transmission of 75%.

solution of PPA is shot by the 8-ns, 532-nm laser light, the transmitted fluence linearly increases in the region of low incident fluence (linear transmittance 75%). The output starts and continues to deviate from the linear-transmission line from the input by about 1.7 J cm^{-2}, implying that the intense illumination gradually bleaches the PPA to transparency, probably by the laser-induced photolysis of the main chains. The PPA/CNT solutions, however, respond to the optical pulses in a strikingly different way. The linear transmittance of a dilute PPA/CNT solution (0.4 mg ml^{-1}) is only 57% (Figure 1.18a), although its concentration is only one-tenth of that (4 mg ml^{-1}) of PPA, probably because of the optical losses caused by the nanotube absorption and scattering. As the incident fluence increases, the PPA/CNT solution becomes opaque, instead of transparent, with its transmitted fluence eventually leveling off or saturating at 1.85 J cm^{-2} (saturation fluence). Clearly, the CNTs have endowed the PPA/CNT with optical limiting power. While PPA is liable to photolysis, the PPA/CNT is stable at very high incident fluence. The energy-sinking and radical-trapping functions of aromatic rings often protect polymers from photodegradation, and the extensively conjugated graphitic aromatic system of the CNTs may have enhanced the resistance of the main chains of PPA against the harsh laser irradiation. As the concentration of the PPA/CNT solution increases, its saturation fluence decreases. Increasing the concentration to 0.6 mg ml^{-1} readily decreases the saturation fluence to as low as 0.45 J cm^{-2}. Similarly, the **72**/C$_{60}$ also effectively limits the strong laser pulses. Compared to the solution of the parent C$_{60}$, the **72**/C$_{60}$ solutions show higher or same linear transmittance but lower saturation fluence [83].
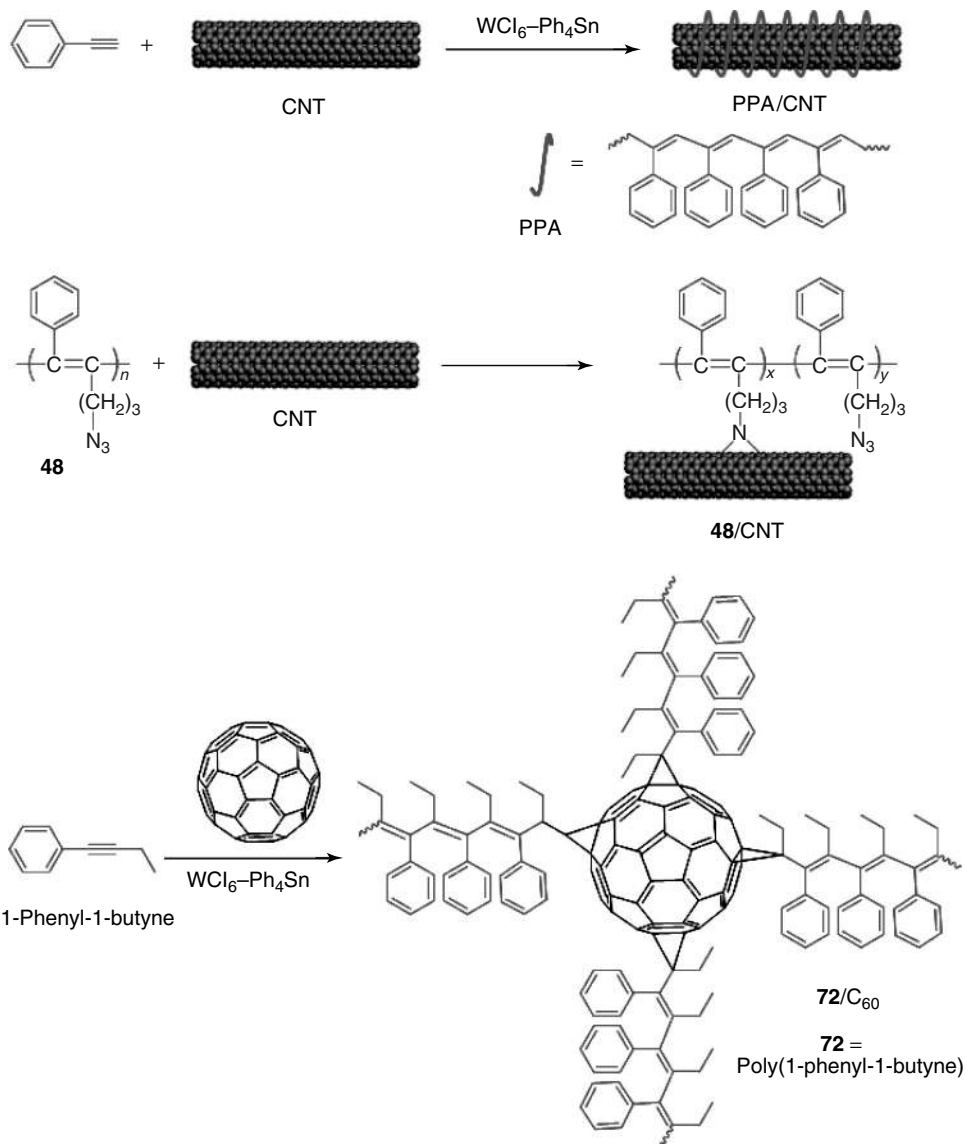
Scheme 1.8 Nanohybridizations of CNT and C_{60} with polyacetylenes.

Much effort has been devoted to the development of second-order NLO materials, particularly to the efficient translation of large molecular first hyperpolarizability to high second harmonic generation (SHG) coefficient (d_{33}). The greatest obstacle in the area has been the chromophoric aggregation in the thin solid films. The NLO dyes are usually highly polarized by the D–A push–pull interactions. During the film formation, the chromophores with large dipole moments tend to compactly

Figure 1.18 (a) Optical limiting responses to 8-ns, 532-nm laser light, of THF solutions of the PPA/CNT hybrid shown in Scheme 1.8. Concentration (c; mg ml^{-1})/linear transmittance (T; %): 0.4/57 (●), 0.5/48 (▲), 0.6/34 (◆). The optical limiting responses of a THF solution of PPA are shown for comparison (c (mg ml^{-1})/T (%): 4.0/75 (○)). (b) Optical limiting responses of a toluene solution of C_{60} (○) and THF solutions of **72**/C_{60} (● and ▲); c (mg ml^{-1})/T (%): 0.16/43 (○), 1.50/56 (●), 3.00/43 (▲).

pack owing to the strong intermolecular electrostatic interactions, leading to the diminishment or cancellation of the NLO effects in the solid state. Researchers have been working on the development of different strategies to overcome this thorny aggregation problem.

Attachment of azobenzene pedants to part of the chain segments of a disubstituted PA may help alleviate the problem because, in addition to the twisted polyene backbone, the chain segments without the azobenzene pendants may serve as isolation buffers to hamper the aggregate formation of the NLO chromophores. It is, however, difficult to synthesize disubstituted PAs with polar azobenzene pendants because of the lack of efficient catalyst systems. We have taken a polymer-reaction approach to prepare the polymers inaccessible by the direct polymerizations. For example, utilizing click reaction, we have successfully synthesized disubstituted PAs with varying contents of functional azobenzene groups, examples of which are shown in Scheme 1.9. As expected, the resultant PAs (**75**) exhibited high d_{33} values (up to ∼130.5 pm V^{-1}) [19].

1.3.10
Biological Compatibility

Decorating the PA backbones with the pendants of naturally occurring building blocks may impart biocompatibility to the π-conjugated polymers. The wrapping of the unnatural polymer chains by the natural molecular coats may result in the ''naturalization'' of the synthetic polymers, thereby generating cytophilic molecular
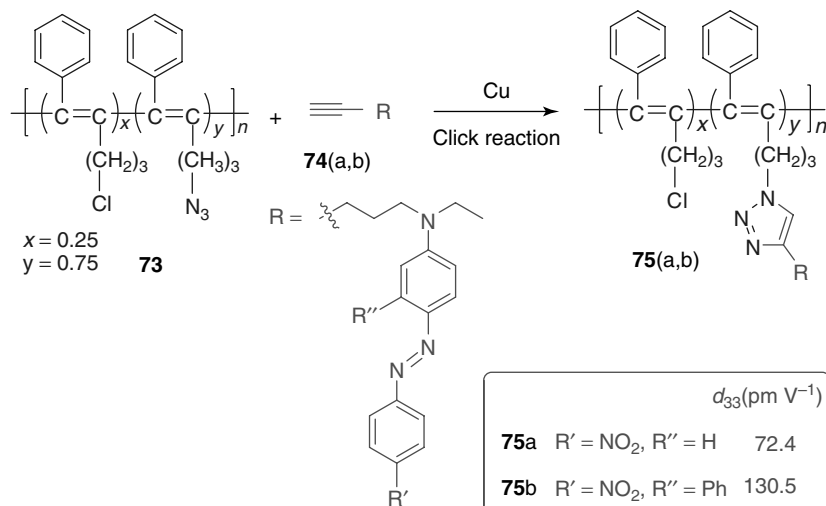
Scheme 1.9 NLO-active polyacetylenes.
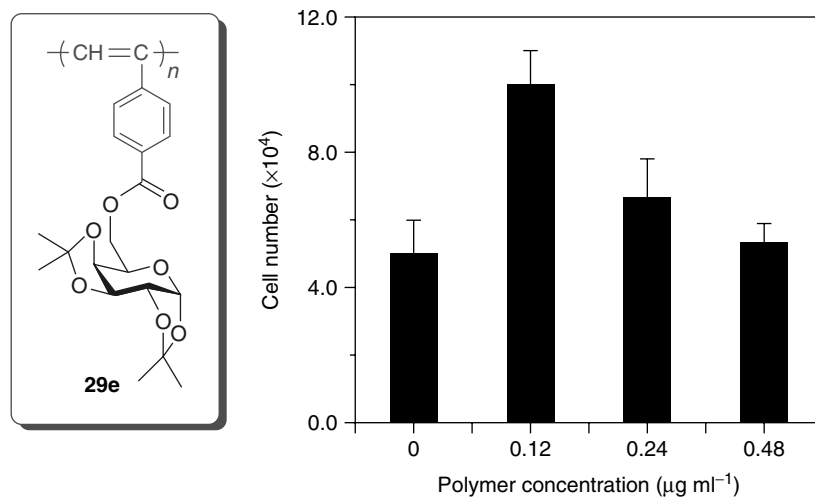
Figure 1.19 Growth of living HeLa cells in the incubation media containing **29e** with different concentrations.

wires. We have systematically investigated the cytotoxicity of a series of PPA derivatives bearing pendant groups of natural origin (amino acids, sugars, nucleosides, etc.) and found them all biocompatible. The bioactivity data for a sugar-containing PPA derivative (**29e**) are plotted in Figure 1.19 [84]. The HeLa cells were subcultured onto the microtiter plates, into which a THF solution of **29e** was added a few hours after the cells had been seeded. The cells were stained with trypan blue and counted with a hemocytometer. As can be seen from Figure 1.19, in the presence of a
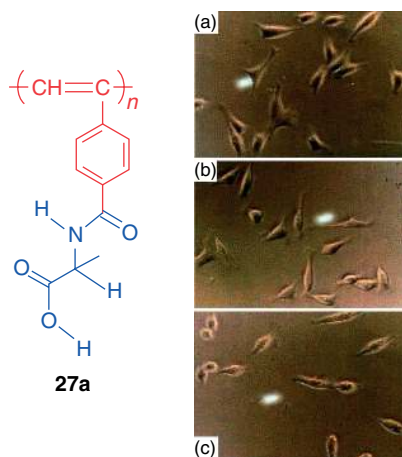
Figure 1.20 HeLa cell adhesion to the microtiter plates precoated with different amounts of **27a** ($\mu g\,cm^{-2}$): (a) 0 (control), (b) 15.8, and (c) 22.2. Incubation time: one day.

small amount of polymer **29e**, the cells grow faster. At a polymer concentration of $0.12\,\mu g\,ml^{-1}$, the cell population is 20-fold higher than that of the control, in which the polymer concentration is zero, although the cell growth returns to normal when the polymer concentration is increased. This indicates that the polymer is cytophilic and can stimulate the growth of the living cells at a low feed.

Figure 1.20 shows the biocompatibility data of a PPA derivative decorated by L-alanine pendants (**27a**) [69]. The HeLa cells were subcultured onto the microtiter plates precoated with polymer **27a**, and the adhesion and growth of the living cells were observed with an optical microscope. After incubation for one day, the cells were found to adhere to, and grow on, the plates as they did in the control experiment, in which the plates without the polymer coatings were used. The polymer exhibited no toxicity to the cells; in other words, it was biocompatible. Even when the polymer coating density was increased to as high as $\sim\!22\,mg\,cm^{-2}$, no dead cells were found throughout the experiment, demonstrative of excellent cytocompatibility of the polymer. Similar results were obtained for the PPA derivatives carrying other amino acid pendants, such as **25a** and **76** (Figure 1.21). This proves that the incorporation of naturally occurring building blocks into the PA structure is a versatile strategy for conferring biocompatibility on the conjugated polymers.

1.4
Conclusions and Prospects

In this work, a large variety of functional moieties are integrated into the molecular structure of PA by the direct polymerizations of functional monomers and the
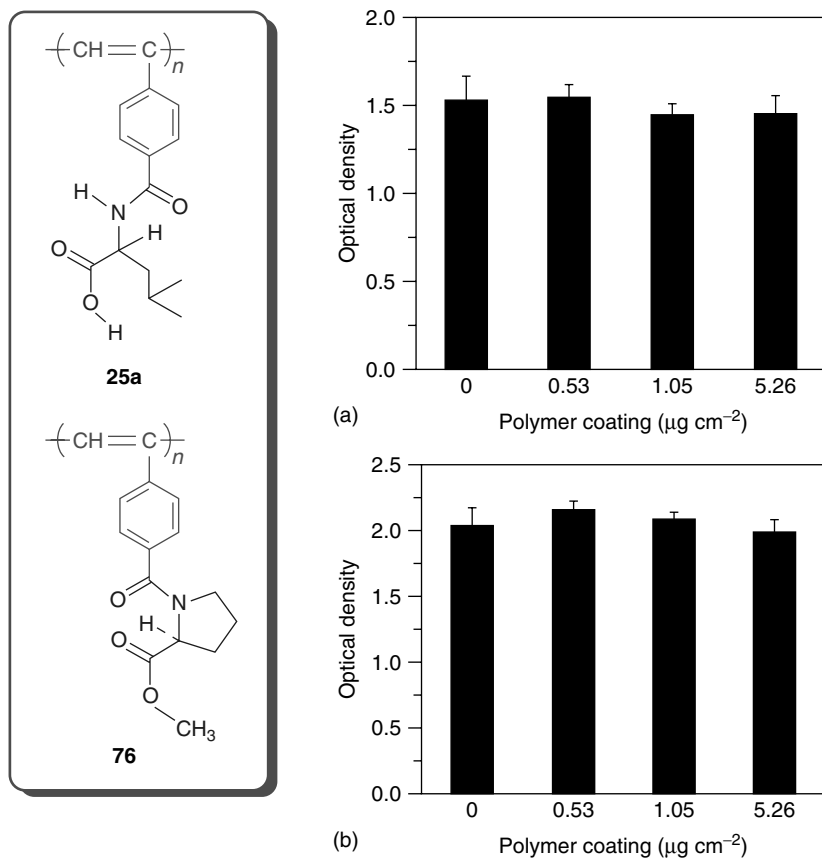
Figure 1.21 Growth of HeLa cells on the microtiter plates precoated with (a) **25a** and (b) **76** after three-day incubation.

polymer reactions of preformed polymers. The functionalization routes explored and the structural insights gained in this study offer versatile synthetic tools and valuable designer guidelines for further developments in the area. Our success in the polymer synthesis proves that the conjugated polyene backbone can be used as a new structural scaffold for the construction of novel functional macromolecules.

The conjugated backbones and functional pendants as well as their synergistic interplays endow PA with an array of unique functionalities. The mesogenic pendants confer liquid crystallinity on PA, while the polyene backbones allow the LCPA chains to be aligned by simple shearing. The energy transfers between the chromophoric pendants and the conjugated skeletons enable the PL colors and efficiencies of the LEPAs to be tuned by molecular engineering. Some LEPAs enjoy an invaluable AIEE nature and are thus promising candidates for PLED applications. The bulky pendants sheath the conjugated skeletons, which weakens chain interactions and boosts spectral stabilities. The chiral pendants induce the

polyene backbones to spiral, with the chain helicity being determined by the pendant chirality. The conformational sensitivity of polyene backbone to environmental surrounding, on the other hand, permits the preferred handedness of their chain segments to be modulated by external perturbations continuously and reversibly. The OAPA chains self-assemble into biomimetic hierarchical structures, thanks to the amphiphilicity stemming from their hydrophobic backbones and hydrophilic pendants. Some substituted PAs with various polarized groups and nanohybrids of PAs with CNT and C_{60} are excellent optical limiting materials. Incorporation of naturally occurring building blocks into the PA structure is a versatile strategy for conferring biocompatibility on the conjugated polymers.

Many of the functionalized PAs are robust and processable, in addition to their simple syntheses and novel functional properties. They may find a wide range of applications as specialty materials in, for example, information storage, photovoltaic cell, chemical sensing, optical display, photoresist pattern, luminescent imaging, optical filtration, nonlinear optics, chiral separation, light polarization, biomimetic morphosynthesis, controlled drug delivery, and tissue engineering. Efforts to exploit the technological applications of the functionalized PAs are currently underway in our laboratories.

Acknowledgments

References

1. Lam, J.W.Y. and Tang, B.Z. (2005) *Acc. Chem. Res.*, **38**, 745.
2. Lam, J.W.Y. and Tang, B.Z. (2003) *J. Polym. Sci., Part A: Polym. Chem.*, **41**, 2607.
3. Masuda, T. (2007) *J. Polym. Sci., Part A: Polym. Chem.*, **45**, 165.
4. Simionescu, C.I. and Percec, V. (1982) *Prog. Polym. Sci.*, **8**, 133.
5. Choi, S.K., Gal, Y.S., Jin, S.H., and Kim, H.K. (2000) *Chem. Rev.*, **100**, 1645.
6. Mayershofer, M.G. and Nuyken, O. (2005) *J. Polym. Sci., Part A: Polym. Chem.*, **43**, 5723.
7. Schrock, R.R., Luo, S.F., Lee, J.C., Zanetti, N.C., and Davis, W.M. (1996) *J. Am. Chem. Soc.*, **118**, 3883.
8. Moore, J.S., Gorman, C.B., and Grubbs, R.H. (1991) *J. Am. Chem. Soc.*, **113**, 1704.
9. Yashima, E., Maeda, K., and Furusho, Y. (2008) *Acc. Chem. Res.*, **41**, 1166.
10. Simionescu, C.I. and Percec, V. (1980) *J. Polym. Sci., Part C: Polym. Symp.*, **67**, 43.
11. Masuda, T. and Higashimura, T. (1984) *Acc. Chem. Res.*, **17**, 51.
12. Furlani, A., Licoccia, S., and Russo, M.V. (1986) *J. Polym. Sci., Part A: Polym. Chem.*, **24**, 991.
13. Yang, W., Tabata, M., Yokota, K., and Shimizu, A. (1991) *Polym. J.*, **23**, 1135.
14. Kishimoto, Y., Eckerle, P., Miyatake, T., Kainosho, M., Ono, A., Ikariya, T., and

Noyori, R. (1999) *J. Am. Chem. Soc.*, **121**, 12035.

15. Tang, B.Z., Poon, W.H., Leung, S.M., Leung, W.H., and Peng, H. (1997) *Macromolecules*, **30**, 2209.

16. Xu, K.T., Peng, H., Lam, J.W.Y., Poon, T.W.H., Dong, Y.P., Xu, H.Y., Sun, Q.H., Cheuk, K.K.L., Salhi, F., Lee, P.P.S., and Tang, B.Z. (2000) *Macromolecules*, **33**, 6918.

17. Law, C.W., Lam, J.W.Y., Dong, Y.P., and Tang, B.Z. (2004) *Polym. Prepr.*, **45**, 839.

18. Yuan, W.Z., Tang, L., Zhao, H., Jin, J.K., Sun, J.Z., Qin, A.J., Xu, H.P., Liu, J.H., Yang, F., Zheng, Q., Chen, E.Q., and Tang, B.Z. (2009) *Macromolecules*, **42**, 52.

19. Zeng, Q., Li, Z., Li, Z., Ye, C., Qin, J., and Tang, B.Z. (2007) *Macromolecules*, **40**, 5634.

20. Zeng, Q., Cai, P., Li, Z., Qin, J.G., and Tang, B.Z. (2008) *Chem. Commun.*, 1094.

21. Tong, H., Lam, J.W.Y., Haussler, M., and Tang, B.Z. (2004) *Polym. Prepr.*, **45**, 835.

22. Xu, H.P., Sun, J.Z., Qin, A.J., Hua, J.L., Li, Z., Dong, Y.Q., Xu, H., Yuan, W.Z., Ma, Y.G., Wang, M., and Tang, B.Z. (2006) *J. Phys. Chem. B*, **110**, 21701.

23. Hua, J.L., Li, Z., Lam, J.W.Y., Xu, H.P., Sun, J.Z., Dong, Y.P., Dong, Y.Q., Qin, A.J., Yuan, W.Z., Chen, H.Z., Wang, M., and Tang, B.Z. (2005) *Macromolecules*, **38**, 8127.

24. Dong, Y.P., Lam, J.W.Y., Peng, H., Cheuk, K.K.L., Kwok, H.S., and Tang, B.Z. (2004) *Macromolecules*, **37**, 6408.

25. Tang, B.Z., Chen, H.Z., Xu, R.S., Lam, J.W.Y., Cheuk, K.K.L., Wong, H.N.C., and Wang, M. (2000) *Chem. Mater.*, **12**, 213.

26. Kang, E.T., Ehrlich, P., Bhatt, A., and Anderson, W. (1984) *Macromolecules*, **17**, 1020.

27. Zhao, H., Yuan, W.Z., Tang, L., Sun, J.Z., Xu, H.P., Qin, A.J., Mao, Y., Jin, J.K., and Tang, B.Z. (2008) *Macromolecules*, **41**, 8566.

28. Yuan, W.Z., Mao, Y., Zhao, H., Sun, J.Z., Xu, H.P., Jin, J.K., Zheng, Q., and Tang, B.Z. (2008) *Macromolecules*, **41**, 701.

29. Yuan, W.Z., Sun, J.Z., Liu, J.Z., Dong, Y.Q., Li, Z., Xu, H.P., Qin, A.J., Haeussler, M., Jin, J.K., Zheng, Q., and Tang, B.Z. (2008) *J. Phys. Chem. B*, **112**, 8896.

30. Yuan, W.Z., Sun, J.Z., Dong, Y.Q., Haussler, M., Yang, F., Xu, H.P., Qin, A.J., Lam, J.W.Y., Zheng, Q., and Tang, B.Z. (2006) *Macromolecules*, **39**, 8011.

31. Xu, H.P., Xie, B.Y., Yuan, W.Z., Sun, J.Z., Yang, F., Dong, Y.Q., Qin, A., Zhang, S., Wang, M., and Tang, B.Z. (2007) *Chem. Commun.*, 1322.

32. Ye, C., Xu, G.Q., Yu, Z.Q., Lam, J.W.Y., Jang, J.H., Peng, H.L., Tu, Y.F., Liu, Z.F., Jeong, K.U., Cheng, S.Z.D., Chen, E.Q., and Tang, B.Z. (2005) *J. Am. Chem. Soc.*, **127**, 7668.

33. Lam, J.W.Y., Dong, Y., Cheuk, K.K.L., Luo, J., Xie, Z., Kwok, H.S., Mo, Z., and Tang, B.Z. (2002) *Macromolecules*, **35**, 1229.

34. Lam, J.W.Y., Luo, J., Dong, Y., Cheuk, K.K.L., and Tang, B.Z. (2002) *Macromolecules*, **35**, 8288.

35. Lam, J.W.Y., Kong, X., Dong, Y., Cheuk, K.K.L., Xu, K., and Tang, B.Z. (2000) *Macromolecules*, **33**, 5027.

36. Kong, X., Lam, J.W.Y., and Tang, B.Z. (1999) *Macromolecules*, **32**, 1722.

37. Kong, X. and Tang, B.Z. (1998) *Chem. Mater.*, **10**, 3352.

38. Tang, B.Z., Kong, X., Wan, X., Peng, H., Lam, W.Y., Feng, X.-D., and Kwok, H.S. (1998) *Macromolecules*, **31**, 2419.

39. Huang, Y.M., Lam, J.W.Y., Cheuk, K.K.L., Ge, W.K., and Tang, B.Z. (1999) *Macromolecules*, **32**, 5976.

40. Lam, J.W.Y., Dong, Y., Kwok, H.S., and Tang, B.Z. (2006) *Macromolecules*, **39**, 6997.

41. Chen, J., Xie, Z., Lam, J.W.Y., Law, C.C.W., and Tang, B.Z. (2003) *Macromolecules*, **36**, 1108.

42. Chen, J., Kwok, H.S., and Tang, B.Z. (2006) *J. Polym. Sci., Part A: Polym. Chem.*, **44**, 2487.

43. Luo, J.D., Xie, Z.L., Lam, J.W.Y., Cheng, L., Chen, H.Y., Qiu, C.F., Kwok, H.S., Zhan, X.W., Liu, Y.Q., Zhu, D.B., and Tang, B.Z. (2001) *Chem. Commun.*, 1740.

44. Chen, J., Law, C.C.W., Lam, J.W.Y., Dong, Y., Lo, S.M.F., Williams, I.D.,

Zhu, D., and Tang, B.Z. (2003) *Chem. Mater.*, **15**, 1535.

45. Yu, G., Yin, S.W., Liu, Y.Q., Chen, J.S., Xu, X.J., Sun, X.B., Ma, D.G., Zhan, X.W., Peng, Q., Shuai, Z.G., Tang, B.Z., Zhu, D.B., Fang, W.H., and Luo, Y. (2005) *J. Am. Chem. Soc.*, **127**, 6335.

46. Peng, Q., Yi, Y., Shuai, Z., and Shao, J. (2007) *J. Am. Chem. Soc.*, **129**, 9333.

47. Peng, Q., Yi, Y., Shuai, Z., and Shao, J. (2007) *J. Chem. Phys.*, **126**, 114302.

48. Chen, H.Y., Lam, W.Y., Luo, J.D., Ho, Y.L., Tang, B.Z., Zhu, D.B., Wong, M., and Kwok, H.S. (2002) *Appl. Phys. Lett.*, **81**, 574.

49. Tong, H., Hong, Y.N., Dong, Y.Q., Haussler, M., Lam, J.W.Y., Li, Z., Guo, Z.F., Guo, Z.H., and Tang, B.Z. (2006) *Chem. Commun.*, 3705.

50. Hong, Y.N., Haussler, M., Lam, J.W.Y., Li, Z., Sin, K.K., Dong, Y.Q., Tong, H., Liu, J.Z., Qin, A.J., Renneberg, R., and Tang, B.Z. (2008) *Chem. Eur. J.*, **14**, 6428.

51. Cheng, K.H., Zhong, Y.C., Xie, B.Y., Dong, Y.Q., Hong, Y.N., Sun, J.Z., Tang, B.Z., and Wong, K.S. (2008) *J. Phys. Chem. C*, **112**, 17507.

52. Tong, H., Hong, Y.N., Dong, Y.Q., Haussler, M., Li, Z., Lam, J.W.Y., Dong, Y.P., Sung, H.H.Y., Williams, I.D., and Tang, B.Z. (2007) *J. Phys. Chem. B*, **111**, 11817.

53. Dong, Y.Q., Lam, J.W.Y., Qin, A.J., Liu, J.Z., Li, Z., and Tang, B.Z. (2007) *Appl. Phys. Lett.*, **91**, 011111.

54. Qin, A.J., Jim, C.K.W., Tang, Y.H., Lam, J.W.Y., Liu, J.Z., Mahtab, F., Gao, P., and Tang, B.Z. (2008) *J. Phys. Chem. B*, **112**, 9281.

55. Yuan, W.Z., Qin, A.J., Lam, J.W.Y., Sun, J.Z., Dong, Y.Q., Haussler, M., Liu, J.Z., Xu, H.P., Zheng, Q., and Tang, B.Z. (2007) *Macromolecules*, **40**, 3159.

56. Hirayama, F. (1965) *J. Chem. Phys.*, **42**, 3163.

57. Yanari, S.S., Bovey, F.A., and Lumry, R. (1963) *Nature*, **200**, 242.

58. Lam, J.W.Y., Qin, A., Dong, Y., Hong, Y., Jim, C.K.W., Liu, J., Dong, Y., Kwok, H.S., and Tang, B.Z. (2008) *J. Phys. Chem. B*, **112**, 11227.

59. Lam, J.W.Y., Peng, H., Haussler, M., Zheng, R., and Tang, B.Z. (2004) *Mol. Cryst. Liq. Cryst.*, **415**, 43.

60. Tang, B.Z., Poon, W.H., Peng, H., Wong, H.N.C., Ye, X.S., and Monde, T. (1999) *Chin. J. Polym. Sci.*, **17**, 81.

61. Tang, B.Z. and Kotera, N. (1989) *Macromolecules*, **22**, 4388.

62. Li, B.S., Chen, J., Zhu, C.F., Leung, K.K.L., Wan, L., Bai, C., and Tang, B.Z. (2004) *Langmuir*, **20**, 2515.

63. Li, B.S., Cheuk, K.K.L., Ling, L., Chen, J., Xiao, X., Bai, C., and Tang, B.Z. (2003) *Macromolecules*, **36**, 77.

64. Li, B.S., Cheuk, K.K.L., Salhi, F., Lam, J.W.Y., Cha, J.A.K., Xiao, X., Bai, C., and Tang, B.Z. (2001) *Nano Lett.*, **1**, 323.

65. Li, B.S., Cheuk, K.K.L., Yang, D., Lam, J.W.Y., Wan, L.J., Bai, C., and Tang, B.Z. (2003) *Macromolecules*, **36**, 5447.

66. Li, B.S., Kang, S.Z., Cheuk, K.K.L., Wan, L., Ling, L., Bai, C., and Tang, B.Z. (2004) *Langmuir*, **20**, 7598.

67. Cheuk, K.K.L., Lam, J.W.Y., Chen, J., Lai, L.M., and Tang, B.Z. (2003) *Macromolecules*, **36**, 5947.

68. Cheuk, K.K.L., Lam, J.W.Y., Lai, L.M., Dong, Y., and Tang, B.Z. (2003) *Macromolecules*, **36**, 9752.

69. Cheuk, K.K.L., Li, B.S., Lam, J.W.Y., Xie, Y., and Tang, B.Z. (2008) *Macromolecules*, **41**, 5997.

70. Lai, L.M., Lam, J.W.Y., Cheuk, K.K.L., Sung, H.H.Y., Williams, I.D., and Tang, B.Z. (2005) *J. Polym. Sci, Part A: Polym. Chem.*, **43**, 3701.

71. Lai, L.M., Lam, J.W.Y., Qin, A., Dong, Y., and Tang, B.Z. (2006) *J. Phys. Chem. B*, **110**, 11128.

72. Lai, L.M., Lam, J.W.Y., and Tang, B.Z. (2006) *J. Polym. Sci., Part A: Polym. Chem.*, **44**, 6190.

73. Lai, L.M., Lam, J.W.Y., and Tang, B.Z. (2006) *J. Polym. Sci., Part A: Polym. Chem.*, **44**, 2117.

74. Salhi, F., Cheuk, K.K.L., Sun, Q., Lam, J.W.Y., Cha, J.A.K., Li, G., Li, B., Luo, J., Chen, J., and Tang, B.Z. (2001) *J. Nanosci. Nanotechnol.*, **1**, 137.

75. Cheuk, K.K.L., Li, B.S., and Tang, B.Z. (2002) *Curr. Trends Polym. Sci.*, **7**, 41.

76. Yin, S., Xu, H., Su, X., Gao, Y., Song, Y., Lam, J.W.Y., Tang, B.Z., and Shi, W. (2005) *Polymer*, **46**, 10592.

77. Yin, S.C., Xu, H.Y., Su, X.Y., Li, G., Song, Y.L., Lam, J., and Tang, B.Z. (2006) *J. Polym. Sci., Part A: Polym. Chem.*, **44**, 2346.

78. Yin, S.C., Xu, H.Y., Shi, W.F., Gao, Y.C., Song, Y.L., and Tang, B.Z. (2006) *Dyes Pigm.*, **71**, 138.

79. Yin, S.C., Xu, H.Y., Shi, W.F., Gao, Y.C., Song, Y.L., Wing, J., Lam, Y., and Tang, B.Z. (2005) *Polymer*, **46**, 7670.

80. Wang, X., Wu, J., Xu, H., Wang, P., and Tang, B.Z. (2008) *J. Polym. Sci., Part A: Polym. Chem.*, **46**, 2072.

81. Tang, B.Z. and Xu, H. (1999) *Macromolecules*, **32**, 2569.

82. Li, Z., Dong, Y., Haussler, M., Lam, J.W.Y., Dong, Y., Wu, L., Wong, K.S., and Tang, B.Z. (2006) *J. Phys. Chem. B*, **110**, 2302.

83. Tang, B.Z., Xu, H., Lam, J.W.Y., Lee, P.P.S., Xu, K., Sun, Q., and Cheuk, K.K.L. (2000) *Chem. Mater.*, **12**, 1446.

84. Li, B., Zhou, J., Xie, Y., and Tang, B.Z. (2001) *Polym. Prepr.*, **42**, 543.